Reassessing two contrasting Late Miocene-Holocene stratigraphic frameworks for the Pearl River Mouth Basin, northern South China Sea

Ming Su [a, b, c] *, Tiago M. Alves [d], Wei Li [a, b] *, Kan-Hsi Hsiung [e], Zhibin Sha [f], Jinqiang Liang [f], Zenggui Kuang [f], Nengyou Wu [g], Rui Yang [c]

a. School of Marine Sciences, Sun Yat-sen University, Guangzhou Guangdong, 510006, China.
b. Guangdong Provincial Key Laboratory of Marine Resources and Coastal Engineering, Guangzhou Guangdong, 510006, China.
c. Key Laboratory of Gas Hydrate, Chinese Academy of Sciences, Guangzhou Guangdong, 510640, China.
d. 3D Seismic Lab, School of Earth and Ocean Sciences, Cardiff University, Main Building, Park Place, Cardiff, CF10 3AT, United Kingdom.
e. R&D Center for Ocean Drilling Science, Yokohama Institute, JAMSTEC, Yokohama, 2360001, Japan.
f. Guangzhou Marine Geological Survey, Guangzhou Guangdong, 510075, China.
g. Key Laboratory of Gas Hydrate, Ministry of Land and Resources, Qingdao Shandong, 266071, China.
Email of corresponding author (Wei Li): iocasliwei@gmail.com

Highlights

1. We reassess two contrasting Late Miocene-Holocene stratigraphic frameworks for the Pearl River Mouth Basin, northern South China Sea.
2. A depositional setting dominated by mass wasting has resulted in miscalculations of stratigraphic boundaries.
3. Regional unconformities and their correlative surfaces, from the shelf edge to the middle and lower continental slope, are traced on high-resolution seismic data.
4. In the study area, stratigraphic frameworks combining seismic and sequence stratigraphic data are more reliable than biostratigraphic frameworks.

Abstract

This work reassesses two contrasting Late Miocene-Holocene stratigraphic frameworks for the Pearl River Mouth Basin (PRMB), northern South China Sea. Two distinct stratigraphic frameworks based on seismic-stratigraphic (SFI) and biostratigraphic (SFII) data are compared in terms of their applicability and accuracy. In order to stress the differences between both frameworks, major stratigraphic boundaries (T1-base Quaternary and T2-base Pliocene) derived from SFI and SFII were revisited and described. Sedimentation rates estimated for the two frameworks, complemented with published data, indicate that average sedimentation rates and trends for SFI match the regional reference data for Quaternary strata. In terms of well-seismic ties, two allochthonous sedimentary units with similar lithology and grain sizes were identified as comprising fine-grained turbidites at the bottom, and fine-grained sediment failures at the top, revealing widespread mass wasting on the middle to lower continental slope. In such a setting, nannofossil assemblages accumulated on the continental slope were likely reworked because of their relatively minute sizes. Sediment cores with low recovery rates collected during a first hydrate expedition in 2007 have led to important misunderstandings when defining the first and last appearances for nannofossil species. Hence, stratigraphic framework I (SFI) - based on a combination of seismic and sequence stratigraphic data - is suggested as more suitable to attain stratigraphic correlations across the continental slope of the PRMB. Our findings can resolve the ambiguities and uncertainties arising from the two contrasting stratigraphic frameworks, providing a robust foundation to reassess the tectono-sedimentary evolution of the PRMB, South China Sea.

Keywords: South China Sea; Pearl River Mouth Basin; Stratigraphic correlation; Stratigraphic boundaries; Late Miocene-Holocene, Submarine canyons.

1. Introduction

Stratigraphic boundaries of chronostratigraphic significance are commonly recorded on borehole and core data as changes in acoustic impedance, seismic-, electro- and lithofacies, presenting distinct biostratigraphic records above and below (Van Wagoner et al., 1987; Hardenbol et al., 1993; Catuneanu, 2006). Hence, the integration of seismic, lithological and biostratigraphic data allows not only a better recognition of stratigraphic boundaries, but also a better grasp of the regional geological history of a sedimentary basin when compared with using either method alone (Loutit et al., 1983; Van Wagoner et al., 1990; Haq, 1991; Catuneanu et al., 2009). High-resolution seismic and borehole data, together with detailed outcrop descriptions, have improved the practical frameworks for stratigraphic correlations adopted by industry and academia, providing important information on sedimentary processes acting in the deep-marine realm, and how these processes are controlled by regional tectonics, eustasy and rates of sediment supply (Johnson et al., 2001; Yoon et al., 2003; Miller et al., 2008; Flint et al., 2011; Lin et al., 2018; Patruno et al., 2018).

The Pearl River Mouth Basin (PRMB) is one of the largest sedimentary basins on the northern continental margin of the South China Sea, and has been the focus of exploration and academic drilling for the past two decades, e.g. ODP Leg 184, IODP Legs 349, 367 and 368 (Fig. 1a). Data from two drilling sites completed during ODP Leg 184 (Sites 1146 and 1148; Fig. 1a), in the southeastern part of the PRMB, were initially used by academia and industry to investigate the tectono-sedimentary evolution of the northern continental margin of the South China Sea (Wang et al., 2000). Particular interest in the continental slope of the PRMB has continued after the discovery of a deep-water gas field near well LW3-1 (Pang et al., 2007; Zhu et al., 2009), near large gas hydrate fields (Wu et al., 2008; Yang et al., 2008, 2015a) (Fig. 1a). Abundant 2D/3D seismic data and two industrial boreholes (BY6-1-1 and LW3-1-1, Fig. 1b) have therefore been acquired on the continental slope of the PRMB for the past 20 years by China National Offshore Oil Corporation (CNOOC). In parallel, regional 2D seismic lines were acquired by the Guangzhou Marine Geological Survey (GMGS) in the mid-2000s to determine and map the distribution of gas hydrates in the PRMB. A pseudo-3D seismic survey derived from 2D seismic data was completed in the target area for gas hydrates (GMGS01) in 2007, where the first marine gas hydrate expedition in China was organized (Wu et al., 2008; Yang et al., 2008) (Fig. 1b).

Against a backdrop of ever-increasing interest in the PRMB, two contrasting Late Miocene-Holocene stratigraphic frameworks have been alternatively used in the published literature. Three major stratigraphic boundaries are considered in these stratigraphic frameworks and named as T1 (base Quaternary), T2 (base Pliocene) and T3 (base Late Miocene) (Fig. 2). Stratigraphic boundaries T1 to T3 were originally traced using regional seismic data when the first stratigraphic framework was proposed for the PRMB (e.g., Pang et al., 2007; Wu et al., 2009; Su et al., 2012; Sun et al., 2012; Li et al., 2013; Yu et al., 2014; Zhou et al., 2015). Such a framework was based on seismic and sequence stratigraphic data and is herein called Stratigraphic Framework I (SFI) (Fig. 2).

A relatively new framework based on biostratigraphic correlations amongst low-recovery sediment cores collected during expedition GMGS01 (Chen et al., 2009; 2013), is named in this work as Stratigraphic Framework II (SFII) (Fig. 2). The SFII has been recently adopted by multiple studies concerning the continental slope of the PRMB (e.g., Wang et al., 2011a, 2011b, 2014a, 2014b; Zhu et al., 2013; Zhou et al., 2015), but there is a blatantly difference in the depth of T1 and T2 at drilling site SH2 when applying the two stratigraphic frameworks SFI and SFII (Fig. 2b). Using SFI, the depths of T1 and T2 are respectively ~221 and ~290 meters below the sea floor (mbsf). Conversely, the depths of these same boundaries in SFII are relatively shallow, i.e. ~57 and ~151 mbsf (Fig. 2b). Despite the obvious differences in the position of stratigraphic boundaries when applying SFI and SFII (Fig. 2), it is a known fact that both the old framework (SFI) and the relatively new framework (SFII), have been concurrently used in the published literature. Confusion between these two contrasting stratigraphic frameworks can lead to: a) disparate regional correlations, and b) erroneous calculations of thickness and sedimentation rates for Late Miocene-Holocene strata. It will also result in serious misunderstandings concerning the Late Cenozoic depositional evolution of the PRMB.

In order to resolve the ambiguities resulting from the concomitant use of SFI and SFII, we focus this work on reassessing these two contrasting stratigraphic frameworks (Fig. 1). Our work describes the character of major unconformities spanning from the shelf edge and upper slope areas of the PRMB, in the north, to middle- to lower- slope regions with slope-confined submarine canyons in the south. We document the differences between SFI and SFII at four hydrate drilling sites not only in terms of the depth(s) of major stratigraphic boundaries, but also considering the trends of average sedimentation rates from Late Miocene to the Quaternary. In addition, sedimentary units sampled at gas hydrate drilling sites are analysed and tied to seismic reflection data. Comparisons between average sedimentation rates, and spatial variations in unconformities within two sedimentary units above BSRs (bottom simulating reflectors), were used to understand which of the two contrasting stratigraphic frameworks (SFI and SFII) is valid for the study area. Our study is of great significance to improve the current regional stratigraphic frameworks applied in the PRMB. It also provides a robust foundation to reassess the regional tectono-sedimentary evolution of the South China Sea.

2. Regional background

2.1 Geological setting

The study area is part of the northern South China Sea, between the Xisha Trough and the Dongsha Islands (Fig. 1a). To the northwest is the Pearl River Delta and to the southeast is the Pearl River Canyon cf. Ding et al. (2013) (Fig. 1a). In this region, the continental slope has a NE-SW orientation and shows an average gradient of 2° (Qiao et al., 2015). The Northwest Sub-basin is located in the southern part of the study area at a water depth of ~ 3500 m (Fig. 1a). Tectonically, the study area is a part of the Baiyun Sag of the Zhu II Depression, within the PRMB (Wu et al., 2011), one of the key hydrocarbon-rich basins in the northern South China Sea. Based on the tectonic evolution of the PRMB, deep-water environments predominated in the study area since, at least, the Middle Miocene (Ru and Pigott, 1986), with regional tectonic

subsidence being associated with the Dongsha and Taiwan tectonic events (Sun et al., 2012; Yu et al., 2014).

The Pearl River is one of the largest rivers in Southeast Asia and comprises a major sediment source to the northern continental margin of the South China Sea. Sediment transported by the PRMB formed the large Pearl River Subaqueous Delta (Fig. 1a), a large delta to prodelta unit characterized by the deposition of large swathes of stacked clinoforms on the continental shelf and upper slope (Lüdmann et al., 2001; Pang et al., 2007; Chen et al., 2014; Zhou et al., 2015). During the Quaternary, the relative large input of sediment from the Pearl River, along with relative sea-level lowstands (Lüdmann et al., 2001), allowed for the development of multiple submarine canyons and deep-water channels on the continental slope of the PRMB. In the study area, linear V-shaped canyons are the most prominent seafloor features (Fig. 1b), most of which show widths of 1-2 km, lengths varying from 20 to 50 km, and a maximum relief of ~ 400 m (Li et al., 2016). Based on the interpretation of high-resolution bathymetric data, these linear canyons are shown to be SSE trending, roughly perpendicular to the continental slope (Fig. 1b). Seventeen submarine canyons are thus observed on the upper continental slope at a water depth between 400 and 700 m, terminating on the lower continental slope at a water depth of about 1200 to 1700 m (Fig. 1b).

2.2 Published stratigraphic frameworks for the PRMB (SFI and SFII)

In previous work, the absolute ages of stratigraphic boundaries T1, T2 and T3 were estimated as 1.8-2.0 Ma, 5.3-5.5 Ma and 10.5-11.6 Ma, respectively (Pang et al., 2007; Chen et al., 2009, 2013; Wu et al., 2009; Sun et al., 2012; Li et al., 2013; Wang et al., 2014b; Yu et al., 2014; Zhou et al., 2015). In this study, the ages of stratigraphic boundaries T1, T2 and T3 were considered as 1.8 Ma, 5.3 Ma and 10.5 Ma in order to compare average sedimentation rates with the regional references later described in section 5.1. The three stratigraphic boundaries considered in our work show minor shifts from the latest International Chronostratigraphic Chart (v 2014/02, URL: http://www.stratigraphy.org/ICSchart/ChronostratChart2014-02.pdf), which defines T1 as 2.58 Ma, T2 as 5.333 Ma, and T3 as 11.62 Ma, respectively.

2.2.1 Stratigraphic framework I (SFI)

Major stratigraphic boundaries in SFI are based on ODP Sites 1146 and 1148 from southeast PRMB (Wang et al., 2000; Lüdmann et al., 2001; Zhao et al., 2001; Clift et al., 2002), and are further interpreted across regional seismic data acquired by CNOOC and GMGS (Li et al. 2013; Zhou et al. 2015; Jiang et al., 2017). Following SFI, stratigraphic boundary T1 was exactly traced at the shelf edge and upper slope, comprising the base of an interval with a set of isochoric, moderate-amplitude continuous seismic reflections (blue double-headed arrows in Fig. 3). At places, stratigraphic boundary T1 is associated with small-scale erosional surfaces, such as those generated by small-scale submarine channels, and is overlain by prograding wedge-shaped, continuous, moderate- to high-amplitude strata (Fig. 3). These prograding seismic reflections are interpreted as shelf-edge deltaic deposits and associated clinothems resulting from abundant sediment transport from the Pearl River (Li et al., 2013; Zhou et al., 2015; Jiang et al., 2017).

Similar isochoric, moderate-amplitude continuous seismic reflections mark stratigraphic boundary T2 on SSE-trending

seismic profiles. Stratigraphic boundary T2 is shown as a relative flat, continuous reflector that follows the slope gradient (Fig. 3). As also documented by Zhou et al. (2015) and Jiang et al. (2017), T1 and T2 correspond at places to the erosional surfaces shown in Figs. 2a and 3.

2.2.2 Stratigraphic framework II (SFII)

Based on sediment cores acquired during the GMGS01 expedition of 2007, a total of 612 samples from four hydrate drilling sites (SH1, SH2, SH5 and SH7) were collected and analysed so that calcareous nannofossil datings could be extracted from the cored strata (Chen et al., 2009; 2013). Following the pioneer studies of Martini (1971) and Okada and Bukry (1980), seventeen calcareous nannofossil events could be determined from these samples (Chen et al., 2013).

Using biostratigraphic data as the basis for a new stratigraphic framework (SFII), the depths of stratigraphic boundaries T1 and T2 were defined as corresponding to distinct nannofossil events (Chen et al., 2013) (Fig. 3). However, due to the fact that the collected sediment cores are essentially discontinuous, and show low recovery rates (about 30% at site SH1), the last occurrence (LO) of *D. brouweri* was difficult to recognise, and the depth of the first occurrence (FO) of *Gephyrocapsa spp.* (>3.5 μm) was subsequently proposed to be the depth of stratigraphic boundary T1 for SFII (Chen et al. 2013). Stratigraphic boundary T2 was considered to be the depth of FO of *C. acutus* (Fig. 4; Table 1). Importantly, these two relatively shallow stratigraphic boundaries (T1 and T2) show no marked changes in seismic-reflection character when projected into the SSE-striking seismic profile crossing hydrate drilling site SH2 (Fig. 2a). In fact, both of these two boundaries are virtually untraceable, as they are correlated with convoluted reflections through the interpreted seismic profiles (Fig. 2a) (see also Figure 8 in Zhou et al., 2015).

2.3 Contemporary use of SFI and SFII

Stratigraphic boundaries T1 and T2 of SFI can be clearly identified on the continental shelf of the PRMB (Li et al., 2013; Zhou et al., 2015; Jiang et al., 2017). However, their depth can only be speculated in the middle to lower continental slope, where submarine canyons are well developed. Here, Upper Miocene-Holocene strata were deeply eroded by submarine canyons, associated submarine channels, and widespread slope instability features (He et al., 2014; Chen et al., 2016; Su et al., 2016). Only sparse geological information from two exploration wells (BY6-1-1 and LW3-1-1, Fig. 1b) can be used to calibrate T1 and T2, in part because these two wells targeted deeper reservoirs and hydrocarbon source intervals. Therefore, based on the biostratigraphic datings from the hydrate drilling sites, SFII has been accepted by some scholars as valid for the middle to lower continental slope of the PRMB (Wang et al., 2011a, 2011b, 2014a, 2014b, 2016; Zhu et al., 2013; Zhou et al., 2015). Clearly, one of the key issues for SFII that needs to be addressed is how to trace stratigraphic boundaries T1 and T2 on seismic data that present no obvious reflections for these two boundaries (Figs. 2c and 2d).

3. Data and methods

High-resolution 2D seismic data acquired by the GMGS were shot using a 3000 m long streamer with 240 channels, a trace interval of 12.5 m, and a tuned air-gun source with a total volume of 8 × 20 in^3 shooting every 25 m. The sampling interval was 1 ms. The streamer depth was 8 m and the source depth 5 m (Wang et al., 2011b). In the target

region for gas hydrates (GMGS01, Fig. 1b), a pseudo-3D seismic survey (e.g. Vanneste et al., 2008), with an area of approximately 9.3 km × 7 km, was acquired by the R/V FENDOU SI HAO of GMGS in 2006 (Wang et al., 2014a). These pseudo-3D seismic data were processed with a sampling interval of 1 ms and a bin size of 12.5 m × 25 m for their inline and crossline directions, respectively (Li et al., 2012).

In this study, one traverse pseudo-3D seismic profile crossing hydrate drilling site SH2, together with a NW-SE 2D seismic profile, are used to illustrate the differences in depth of key stratigraphic boundaries when considering SFI and SFII (Fig. 2a). Seven 2D seismic profiles are used in this work to image the area spanning the shelf-edge/upper continental slope to the lower slope and basin floor (Figs. 4a, 4c, 5a, 6a, 6b, 7a and 7b).

Two pseudo-3D seismic profiles are used to image the two units above BSRs sampled by low-recovery rates cores at the hydrate drilling sites (Fig. 8). All the seismic lines presented in this study are shown in two-way travel time (TWTT). Published stratigraphic correlations for the Shenhu Area - based on seismic and biostratigraphic data - were reassessed in this study. To identify and describe seismic facies, our approach was mostly based on the recognition of key seismic characteristics such as reflection frequency, amplitude, continuity and the geometry of reflection terminations (onlap, downlap and erosional truncations).

The GMGS01 expedition was undertaken in collaboration with Fugro and Geotek, onboard the M/V *Bavenit*, using a Fugro Hydraulic Piston Corer (FHPC) and a Fugro Corer (FC). A Fugro Pressure Corer (FPC) and a Fugro Rotary Pressure Corer (FRPC) were also used to obtain core samples at four shallow drilling sites located between canyons SC9 to SC11 (sites SH1, SH2, SH5 and SH7, Fig. 1b) without releasing *in situ* pressures. The deepest core retrieved was SH2, which reached a depth of about 242 mbsf. At site SH7, about 116 samples were used for grain-size analysis (Fig. 9). A total of 14 samples were taken between 155 mbsf and 176.7 mbsf, where gas hydrates were recovered, while the remaining 102 samples were collected at depths ranging from 0.1 mbsf to 155 mbsf in sediment lacking gas hydrates. In the study area, two hydrocarbon exploration boreholes were also drilled by the China National Offshore Oil Corporation (CNOOC) (BY6-1-1 and LW3-1-1, Fig. 1b) so as to determine the characteristics of source rocks and reservoirs intervals in the Baiyun Sag, PRMB.

Stratigraphic boundary T3, the base of Upper Miocene strata, is documented in the study area as the base of unidirectionally migrating channels (Zhu et al., 2010; Lü et al., 2012; Ding et al., 2013; Gong et al., 2013; Li et al., 2013; Zhou et al., 2015; Ma et al., 2015). It is currently accepted by both SFI and SFII. A power time-depth function for the PRMB, introduced by Zhou et al. (2008), was used to obtain the depths of boundary T3, and boundaries T1 and T2 of SFI at the four hydrate drilling sites (Table 1). The depths of major stratigraphic boundaries for SFII were obtained through the identification of calcareous nannofossil biostratigraphic events from these low-recovery sediment cores (Chen et al., 2013) (Fig. 3 and Table 1).

4. Results and interpretation

4.1 Seismic facies analysis

Small-scale erosional features

Following SFI at the shelf of the PRMB – similarly to the approach taken by Zhou et al. (2015) and Jiang et al. (2017) - prograding shelf-edge deltas and clinothems can be

interpreted on the SSE-striking profiles (Figs. 4a and 5a). Based on their internal seismic architecture, the prograding complexes can be divided into sub-sequences alternating with gravity-flow deposits of high amplitude (Fig. 4b) (see also Figure 8 in Jiang et al., 2017), and mass-transport deposits (MTDs) with chaotic, high-amplitude seismic reflections (Fig. 5b). From the shelf edge to the upper continental slope, stratigraphic boundary T1 of SFI comprises the base of an interval with a set of isochoric, moderate-amplitude continuous seismic reflections (Figs. 4a and 5a). Further southeast, close to the headwall areas of submarine canyons, several high-amplitude reflections can be observed (Figs. 4b and 5c). Projected into the NEE-striking seismic section on the upper continental slope, these irregular high-amplitude reflections (Fig. 4b) correspond to the erosional bases of small-scale submarine channels in Fig. 4c. On other NEE-striking seismic profiles (e.g. Fig. 6a), a series of small-scale submarine channels can be recognised with a width of about 1-4 km.

On the upper continental slope, the down-cutting depth of small-scale erosional features is relatively shallow, about 50-200 ms TWTT (Figs. 4c, 5c and 6a). In similarity to what is observed on the shelf edge (Fig. 4b), small-scale erosional features on the upper continental slope are draped by isochoric, continuous moderate-amplitude reflections (Figs. 4c and 6a).

Non-migrating erosional features associated with continuous seismic reflections

Stratigraphic boundary T2 on the continental shelf, documented by Zhou et al. (2015) and Jiang et al. (2017), coincides with the base of a set of isochoric, moderate-amplitude continuous seismic reflections on the SSE-striking seismic sections (Fig. 4b). On the continental slope these flat, continuous reflections are disturbed by thick transparent to moderate-amplitude strata, which alternate with chaotic high-amplitude seismic reflections (Fig. 4a).

Previous studies in the PRMB have identified unidirectionally migrating channels on the continental slope (Zhu et al., 2010; Lü et al., 2012; Ding et al., 2013; Gong et al., 2013; Li et al., 2013; Zhou et al., 2015; Ma et al., 2015), the bases of which are considered to be stratigraphic boundary T3 (11.62 Ma, Late Miocene). Migrating channels are clearly observed in the zoomed in seismic section in Fig. 4d. On the southern part (middle to lower continental slope) of the SSE-striking seismic profile in Fig. 5a, these migrating channels are eroded by high-amplitude seismic reflections, and overlain by a set of continuous, moderate-amplitude seismic reflections. On the zoomed in seismic section in Fig. 5c, the base of the migrating channels coincides with an erosional surface draped by continuous, moderate-amplitude seismic reflections. On the NEE-striking seismic profiles, U-shaped morphologies and sub-parallel to lenticular, high-amplitude reflections are visible near the base of the channels (Figs. 6a and 6b). According to the geological model proposed by Mayall et al. (2006), these high-amplitude seismic reflections are channel-lag deposits at the base of thalwegs (Figs. 6c and 6d), similar to the deposits studied in Zhu et al. (2010). In some areas, NEE-striking seismic profiles do not reveal migrating channels below these erosional surfaces (Figs. 6a and 6b). Also in NEE-striking profiles, a set of continuous seismic reflections with moderate amplitude is recognised - the erosional features associated with continuous seismic reflections reveal the break-off surface for the migrating channels (Figs. 5a, 6a and 6b).

Enveloping surfaces of turbidites within the submarine canyons

On the middle to lower continental slope, sub-parallel to chaotic, high-amplitude seismic reflections are interpreted as turbidites within SC8 (Fig. 5a) and SC5 (Fig. 7a). The enveloping surfaces of discrete submarine canyons can also be recognised.

Erosional truncations

In Fig. 7, erosional truncation is obvious near non-migrating erosional channels. On the upper continental slope, continuous and oblique seismic reflections are truncated by a set of isochoric moderate-amplitude reflections (Figs. 7a and 7b). On the middle to lower continental slope, these continuous high-amplitude seismic reflections show continuous moderate- to high-amplitude seismic reflections with prograding geometries (Figs. 4 and 7). These prograding seismic reflections are truncated on their top on multiple parts of the continental slope (Fig. 7a).

4.2 Units identified in low-recovery sediment cores from hydrate drilling sites

Low-recovery sediment cores obtained at the hydrate drilling sites of expedition GMGS01 comprise silt and silty clay (Chen et al., 2011, 2013). Hydrate-bearing deposits at the bottom of the cores (195-220 mbsf at site SH2, and 155-176.7 mbsf at site SH7), reported by Chen et al. (2011) and Liu et al. (2012), are similar to deposits without hydrates in terms of their lithology and grain size.

Two pseudo-3D seismic profiles crossing the hydrate drilling sites were tied to stratigraphic data collected above BSRs (Fig. 8). In the northern parts of the two pseudo-3D profiles (near the middle part of the continental slope), strata above the BSRs can be divided into two units with distinct seismic characters. Thin-bedded, chaotic, high-amplitude seismic reflections with lenticular- to irregular-shaped geometries are identified immediately above the BSRs, and are labelled as Unit I in this work (Figs. 8a and 8b). Above these thin-bedded chaotic reflections, Unit II presents thick continuous moderate-amplitude reflections with wavy geometries (Fig. 8). Unit II is widely distributed in intercanyon areas on the middle and lower continental slope of the PRMB (Figs. 2c, 4a, 6a, 7 and 8).

At the hydrate site SH7, thin-bedded chaotic reflections correspond to hydrate-bearing strata at the bottom of the drilled succession (155-176.7 mbsf), whereas thick continuous seismic reflections correlate with sediment without hydrates towards the top (0.1-155 mbsf). Grain size analyses for 116 samples from site SH7 were used to obtain the scatter plot of one-percentile and median values of grain size; defined as Cm patterns by Passega (1964). From the Cm pattern in Fig. 9, the 116 samples could be divided in two groups. Thirteen (13) samples from hydrate-bearing sediments in Unit I (Fig. 8a) show a linear distribution that is sub-parallel to the C=M baseline (Group I; Fig. 9). The other 102 samples in Unit II (Fig. 8a), show marked differences when compared to Group I sediment (see Group II samples in Fig. 9).

4.3 Differences between SFI and SFII

In the study area, Upper Miocene-Holocene strata can be divided into three main stratigraphic intervals: a) Quaternary, from the sea floor to stratigraphic boundary T1, b) Pliocene, between T1 and T2, and c) Upper Miocene between T2 and T3 (Fig. 10a). Adopting SFI (Table 1), the thickness of these three intervals is estimated as 219 m, 57 m and 249 m at site SH1; 221 m, 69 m and 282 m at site SH2; 181 m, 65 m and

315 m at site SH7; and 172 m, 46 m and 184 m at site SH5 (Fig. 10a). Adding to these estimates, the thickness of the three stratigraphic intervals can also be calculated from SFII (Table 1), comprising about 58 m, 85.7 m and 381.3 m at site SH1; 57 m, 93.85 m and 421.15 m at site SH2; 109 m, 62.2 m and 389.8 m at site SH7; and 96.73 m and 305.27 m for the Pliocene and Upper Miocene intervals at site SH5 (Fig. 10a).

One of the most obvious differences between SFI and SFII lies on the thickness of the Quaternary and Upper Miocene intervals (Fig. 10a). Based on SFI, Quaternary and Upper Miocene strata are relatively thick, varying between 172-221 m and 184-315 m, respectively (Fig. 10a). Conversely, Pliocene strata are relatively thin, with about 46-69 m (Fig. 10a). A thin Pliocene interval can be estimated by SFII, with about 62-94 m in thickness (Fig. 10a). However, compared to SFI, thickness estimates for Quaternary strata using SFII are relatively lower (57-109 m), whereas Upper Miocene sediments are relatively thick, varying between 305-421 m (Fig. 10a).

An important detail is the trend of average sedimentation rates from Late Miocene to Quaternary strata. Sedimentation rates in SFI increase gradually reaching a maximum value of about 8.57 cm/ka at site SH2 during the Quaternary (Fig. 10b). In SFII they decline towards the present day, showing a maximum of about 6.69 cm/ka during the Late Miocene at site SH2 (Fig. 10b).

5. Discussion

5.1 Regional trends for average sedimentation rates from Late Miocene to Quaternary

On the basis of 94 seismic profiles, wireline data from 34 industrial boreholes and 121 sediment cores, Huang and Wang (2006, 2007) calculated average sedimentation rates for the South China Sea from the onset of seafloor spreading (Oligocene) to the present day. Yet, there are some uncertainties in the parameters estimated by Huang and Wang (2006, 2007) due to the variable vertical resolution of the seismic data interpreted by these latter, the rather distinct locations of sediment cores, the absolute estimates of sediment density, and the influence of erosion and compaction in the final estimates of sedimentation rates. Huang and Wang (2006, 2007) results can, nonetheless, be considered as the most reliable benchmark for the PRMB because most exploration wells and sediment cores are located in this area.

Based on our results, average sedimentation rates have gradually increased in the PRMB since the Late Miocene (Fig. 10b). Using the two contrasting stratigraphic frameworks SFI and SFII, the trends of average sedimentation rates can be estimated at the four GMGS01 hydrate drilling sites, for Late Miocene-Quaternary strata. Confirming data in Huang and Wang (2006, 2007), the trends for SFI increase (red arrow in Fig. 5b), recording a maximum average sedimentation rate in the Quaternary. A gradually increasing trend from ~11 Ma to the present day was also postulated by Clift (2006). The relatively high average sedimentation rates recorded in the study area for Quaternary strata are suggestively associated with enhanced sediment input since 2-4 Ma due to global climate change (Zhang et al., 2001), along with relative sea-level lowstands (Lüdmann et al., 2001). As a result, at the shelf edge and upper continental slope of the PRMB, thick shelf-edge deltas and associated clinothems developed during the Quaternary (Figs. 4b, 5b and 7).

5.2 Sedimentary processes of two distinct units documented at hydrate drilling sites

Although sediment above the BSRs

sampled at the GMGS01 hydrate drilling sites is similar in lithology and grain size (Chen et al., 2011; Liu et al., 2012), two different sedimentary units can be recognised on seismic data (Fig. 8) and Cm patterns (Fig. 9).

On the basis of the classification system proposed by Passega (1964), sediment at the bottom of low-recovery cores at site SH7 (corresponding to thin-bedded chaotic reflections on seismic data) comprises turbidites (Fig. 9). As shown on the seismic profiles in Figs. 4c, 5c, 6a and 7b, small-scale channels developed at this time at the shelf-edge and upper continental slope, and form stratigraphic boundary T1 of SFI. In the target area for gas hydrates (GMGS01), stratigraphic boundary T1 of SFI overlaps the BSRs (Sun et al., 2012; Su et al., 2015, 2016), e.g. hydrate drilling site SH2 in Fig. 2a.

Considering as valid the deep-water sedimentary processes reported by previous studies (Stow and Mayall, 2000; Hubbard et al., 2009; Lericolais et al., 2013; Macauley and Hubbard, 2013), we can infer that the thin-bedded fine-grained turbidites deposited in middle to lower slope areas (Unit I in Fig. 8) are associated with small-scale channels developed further north, on the shelf edge and upper continental slope (Su et al., 2015, 2016). Eroded by these small-scale channels, slope strata to the north of the study area were re-transported and re-deposited as thin-bedded fine-grained turbidites on the middle to lower continental slope.

Based on the internal seismic character of Unit II, which comprises original bedding without obvious internal disruption (Figs. 2c-d and 8), the widely distributed continuous, moderate- to high-amplitude wavy reflections in intercanyon areas can be interpreted as submarine landslides (Figs. 2a, 4a, 5a, 6 and 7). As one of the most important deep-water geomorphologic and depositional features on continental margins, submarine landslides are associated with the downslope movement of unconsolidated sediment due to gravitational forces (Mills, 1983; Hampton et al., 1996; Moscardelli and Wood, 2008; Hüneke and Mulder, 2011). From the intersecting SEE-striking seismic profiles, putative submarine landslides were triggered at the front of the shelf-edge delta and associated clinothems (Figs. 4a, 5a and 7). Thick, fine-grained submarine landslides located on the middle to lower continental slope, between submarine canyons, can be considered as resulting from downslope movement of unconsolidated sediment triggered by enhanced sediment supply from the north (Lüdmann et al., 2001; Pang et al., 2007; Zhou et al., 2015). This specific predisposing factor complemented the relative tectonic and depositional steepening of seafloor topography (He et al., 2014; Qiao et al., 2015; Chen et al., 2016), and the local dissociation of gas hydrates (Chen et al., 2016). We can therefore infer that sediment sampled at hydrate drilling sites was redeposited, rather than comprising autochthonous strata.

5.3 Reassessing biostratigraphic framework SFII from low-recovery cores

Strata above the BSRs sampled on the middle to lower continental slope were initially considered as homogeneous fine-grained deposits reflecting similar (and relatively continuous) depositional processes, because the lithology and grain size of samples are similar through the entire length of the cores (Chen et al., 2011; Liu et al., 2012). These results were further considered as the basis for regional biostratigraphic correlations based on low-recovery cores. However, the distinct sedimentary processes identified in this work (low-energy turbidite flows and associated submarine mass wasting) reveal complex depositional processes at the location of the hydrate drilling sites.

Influenced by gravity flows and bottom

currents, the nannofossils collected at the hydrate drilling sites were likely reworked because of their relatively minute grain sizes, making it difficult to truly define first and last appearance datum levels (Ujiié, 1994). As a practical example of this caveat, over 130 reworked calcareous nannofossil taxa, ranging from the Lower Jurassic to the Neogene, have been recorded in Quaternary sediments of the central Arctic Ocean (Gard and Crux, 1994). In parallel, nannofossils from northwest Europe were extensively reworked throughout the last glacial interval and later discharged in the North Atlantic Ocean (Rahman, 1995). At IODP Site U1432C in the Northwest Sub-basin of the South China Sea, nannofossil preservation is moderate to good, but still shows considerable reworking of Pliocene and Miocene species within the Pleistocene Interval at 0-50 mbsf (Expedition 349 Scientists, 2014). Also at IODP Site U1499, to the south of the study area (see location in Fig. 1b), Pleistocene turbidite sequences and slump deposits comprise reworked nannofossils (Expeditions 367 and 368 Scientists, 2017).

Due to the non-uniform distribution of the samples used to identify calcareous nannofossil biozones, the chronostratigraphic dates obtained during GMGS01 should be comprehensively reassessed. As shown in Fig. 3, core recovery at the four hydrate drilling sites is extremely low, with 30% at site SH1, 21% at site SH2, 50% at site SH5, and 26% at site SH7. Sediment cores at the four hydrate drilling sites were continuous at their upper sections, between the seafloor and 20-40 mbsf (Fig. 3). The majority of nannofossil specimens analysed were taken from these sections, at sampling intervals of 0.1 m (Chen et al., 2013). In contrast, a very small number of nannofossil samples were collected below 40 mbsf, and sampling often followed a maximum interval of about 60 m (Fig. 3). As summarised in Fig. 3, the depths of stratigraphic boundary T1 from SFII at sites SH1, SH2 and SH7, were determined with important caveats. The FO of *C. acutus* was not observed at site SH5 and the depth of stratigraphic boundary T2 in SFII was not detected at this same site (Fig. 3). The presence of reworked nannofossils might have been neglected due to the low recovery of these sediment cores, leading to effective biostratigraphic dates that represent the ages of reworked sediment particles rather than their depositional ages. Therefore, against a background of frequently developed mass movements, the biostratigraphic datings based on the calcareous nannofossils collected at the hydrate drilling sites in the PRMB, with low recovery rates, are not appropriate to define major stratigraphic boundaries.

5.4 Vertical variations in erosional features

Zhu et al. (2010) reported for the first time a series of submarine canyons and channels in the PRMB, migrating progressively to the northeast since the Late Miocene, and explained their migration as resulting from the interaction between turbidity and bottom currents. These channels were further described by Lü et al. (2012), Ding et al. (2013), Gong et al. (2013), Li et al. (2013), Zhou et al. (2015), and Ma et al. (2015). Stratigraphic correlations undertaken in the study area reveal important vertical variations in the erosional features generated by submarine canyons and channels. In the NEE-striking profiles across the continental slope, buried migrating channels are observed, and reveal stratigraphic boundary T3 as their base (Fig. 6). Channel-fill deposits with high-amplitude seismic reflections at the top of migrating channels can be interpreted as channel-lag deposits without laterally migrating features (Figs. 6c and 6d). These high-amplitude reflections are overlain by a set of continuous moderate-amplitude strata

(Fig. 6a), similar to those is observed on the shelf edge and upper continental slope (Figs. 5c and 7). A series of small-scale erosional features interpreted as small-scale channels are also overlain by a sediment drape comprising continuous moderate-amplitude reflections (Fig. 6a). Near the modern sea floor, thick continuous moderate/high-amplitude reflectors with wedge shapes (or wavy geometries) correspond to shelf-edge deltas, prograding clinothems and submarine landslides (Fig. 6a), as also observed on SSE-striking seismic sections (Figs. 3a, 5a and 7). On the sea floor, V-shaped slope-confined submarine canyons are developed at present (Fig. 6).

Therefore, four irregular erosional surfaces are clearly observed on seismic data, and comprise angular unconformities. These unconformities indicate four major erosional-sedimentary events since the Late Miocene: a) the incision of laterally migrating channels, b) the draping of submarine channels by sub-parallel strata and cessation of lateral migration in channels, c) the generation of small-scale channels overlain by draping strata, and d) incision of slope-confined submarine canyons (Fig. 6). In the study area, vertical variations in erosional geometries can help identifying major stratigraphic boundaries, as the bases of the four major events correspond to regional unconformities: Stratigraphic boundaries T3, T2 and T1, and the modern sea floor.

5.5 Spatial variations in the character of regional unconformities

Using high-quality seismic data, spatial variations in stratigraphic boundaries T2 and T1 can be traced in different parts of the study area. These two boundaries comprise prominent unconformities at the shelf edge and upper continental slope and are nearly conformable in the middle to lower slope areas, forming parallel unconformities, disconformities or local paraconformities (Figs. 4a and 7b). Therefore, detailed seismic facies analyses should be regarded as crucial to tracing stratigraphic boundaries in the southern half of the study area.

On the middle-lower continental slope, stratigraphic boundary T1 correlates with the base of submarine landslides with wavy continuous reflections (Figs. 4a and 7b), also corresponding to BSRs in the target areas with gas hydrates (GMGS01; Figs. 2a and 8). Variations in seismic character are obvious as wavy moderate-amplitude reflections occur above T1 and chaotic high-amplitude seismic reflections are observed below this same boundary (Fig. 4a). On SEE-striking seismic profiles, in places where the erosional power of submarine canyons was relatively weak, stratigraphic boundary T1 can be identified as a flat continuous moderate-amplitude seismic reflection on the middle to lower continental slope, but correlates with a marked erosional surface on the shelf edge and upper continental slope (Fig. 7b). In intracanyon areas, this stratigraphic boundary is regarded as the base of high-amplitude reflections with U-shaped geometries (Figs. 5a and 7a).

In Late Miocene and Pliocene strata, multiple internal boundaries are observed on the NEE-striking profiles due to multiple cut-and-fill processes (Fig. 6). As shown on SSE-striking profiles, inclined high-amplitude reflections were truncated on the upper and middle continental slope and later draped by a set of isochoric continuous moderate-amplitude reflections (Fig. 5). Stratigraphic boundary T2 is identified here in association with an erosional feature showing no lateral migration in channels (Fig. 6).

On the lower continental slope and basin floor, the truncation surface on top of prograding seismic reflections represents an important erosional unconformity (Fig. 7). Changes in the seismic character are also

obvious, showing a set of isochoric continuous moderate-amplitude reflections above T2 and disturbed moderate-/high-amplitude reflectors below this same boundary (Fig. 7). Spatial variations in stratigraphic boundary T2, from north to south, are observed on SSE-striking seismic profiles to reveal: a) an erosional unconformity at the shelf edge and upper continental slope, b) truncation surfaces draped by moderate-amplitude continuous seismic reflections on the upper and middle continental slopes, and c) paraconformities with variations in seismic facies across this same boundaries on the lower continental slope and basin floor. Hence, unconformities and variations in internal seismic facies are proposed here as supplementary features to identify stratigraphic boundaries T1 and T2 on the lower continental slope.

6. Conclusions

Two contrasting stratigraphic frameworks were revisited by identifying key regional boundaries. Remarkable differences between stratigraphic frameworks based on seismic and sequence stratigraphy (SFI) and biostratigraphy (SFII) are clear when analysing two key stratigraphic boundaries: a) T2 (base of Pliocene) and T1 (base of Quaternary). As a result, we prove that thin-bedded, fine-grained turbidites and thick fine-grained mass-wasting deposits sampled in expedition GMGS01 comprise reworked strata rather than homogeneous fine-grained deposits, though there were no significant changes in lithology and grain size from the bottom to the top of the acquired low-recovery sediment cores. Under sedimentary processes dominated by gravity flows, considerable reworking of calcareous nannofossils should have occurred.

Based on the detailed analysis of seismic data, erosional features generated from stratigraphic boundary T3 (base Late Miocene) to the sea floor indicate four major erosional events affecting the continental slope of the PRMB since the Late Miocene. The bases of migrating submarine channels, channels draped by younger strata, small-scale channels and submarine canyons are proposed to mark the boundaries T3, T2, T1, and the modern sea floor. Unconformities and apparent variations in seismic facies and geometries are suggested as additional diagnostic features of stratigraphic boundaries T1 and T2.

As a corollary, this study shows that stratigraphic boundaries T1 and T2 - based on seismic and sequence stratigraphic data (SFI) - are more suitable than biostratigraphy data from SFII to characterise the evolution of the northern continental slope of the PRMB, northern South China Sea.

Acknowledgements

We would like to thank first and foremost the generosity of Guangzhou Marine Geological Survey (GMGS) for the release of seismic data. Dr. François Bache and Dr. Kamaldeen Omosanya are thanked for their thorough reviews and constructive comments. This study is supported by the National Natural Science Foundation of China (No. 41576048 and 41876054), the Pearl River S&T Nova Program of Guangzhou (No. 201710010198), the Guangdong Special Fund for Economic Development (Marine Economy) (No. GDME-2018D001), and the Scientific cooperative project by CNPC and CAS (RIPED-LFFY-2015-JS-219). Dr. Wei Li is funded by the CAS Pioneer Hundred Talents Program.

References

Catuneanu, O. Principles of Sequence Stratigraphy. Elsevier, Amsterdam, 2006, pp. 375.

Catuneanu, O., Abreu, V., Bhattacharya, J.P., Blum, M.D., Dalrymple, R.W., Eriksson, P.G., Fielding, C.R., Fisher, W.L., Galloway, W.E., Gibling, M.R., Giles, K.A., Holbrook, J.M., Jordan, R., Kendall, C.G.St.C., Macurda, B., Martinsen, O.J., Miall, A.D., Neal, J.E.,

Nummedal, D., Pomar, L., Posamentier, H.W., Pratt, B.R., Sarg, J.F., Shanley, K.W., Steel, R.J., Strasser, A., Tucker, M.E., Winker, C. Towards the standardization of sequence stratigraphy. Earth-Science Reviews, 2009, 92(1-2): 1-33.

Chen, D.X., Wang, X.J., Völker, D., Wu, S.G., Wang, L., Li, W., Li, Q.P., Zhu, Z.Y., Li, C.L., Qin, Z.L., Sun, Q.L. Three dimensional seismic studies of deep-water hazard-related features on the northern slope of South China Sea. Marine and Petroleum Geology, 2016, 77: 1125-1139.

Chen, F., Su, X., Zhou, Y., Lu, H.F., Liu, G.H., Chen, Z.X., Chen, C.Y. Variations in biogenic components of Late Miocene-Holocene sediments from Shenhu Area in the northern South China Sea and their geological implication. Marine Geology & Quaternary Geology, 2009, 29(2): 1-8. (in Chinese with English abstract)

Chen, F., Zhou, Y., Su, X. Liu, C.H., Lu, H.F., Wang, J.L. Gas hydrate saturation and its relation with grain size of the hydrate-bearing sediment in the Shenhu Area of northern South China Sea. Marine Geology & Quaternary Geology, 2011, 31(5): 95-100. (in Chinese with English abstract)

Chen, F., Su, X., Zhou, Y. Late Miocene-Pleistocene calcareous nannofossil biostratigraphy of Shenhu gas hydrate drilling area in the South China Sea and variations in sedimentation rates. Earth Science: Journal of China University of Geosciences, 2013, 38(1): 1-9. (in Chinese with English abstract)

Chen, H., Xie, X.N., Rooij, D.V., Vandorpe, T., Su, M., Wang, D.X. Depositional characteristics and processes of alongslope currents related to a seamount on the northwestern margin of the Northwest Sub-Basin, South China Sea. Marine Geology, 2014, 355: 36-53.

Chen, J.S., Xu, S.C., Sang, J.Y. The depositional characteristics and oil potential of paleo Pearl River delta systems in the Pearl Piver Mouth Basin, South China Sea. Tectonophysics, 1994, 235(1-2): 1-11.

Clift, P., Lee, J.I., Clark, M.K., Blusztajn, J. Erosional response of South China to arc rifting and monsoonal strengthening; a record from the South China Sea. Marine Geology, 2002, 184(3-4): 207-226.

Clift, P. Controls on the erosion of Cenozoic Asia and the flux of clastic sediment to the ocean. Earth and Planetary Science Letters, 2006, 241(3-4): 571-580.

Ding, W.W., Li, J.B., Li, J., Fang, Y.Z., Tang, Y. Morphotectonics and evolutionary controls on the Pearl River Canyon system, South China Sea. Marine Geophysical Research, 2013, 34(3-4): 221-238.

Expedition 349 Scientists. South China Sea tectonics: Opening of the South China Sea and its implications for southeast Asian tectonics, climates, and deep mantle processes since the late Mesozoic. International Ocean Discovery Program Preliminary Report, 349. 2014. http://dx.doi.org/10.14379/iodp.pr.349.2014.

Expeditions 367 and 368 Scientists. South China Sea Rifted Margin. International Ocean Discovery Program, Reports Overview, Expedition Information, Site U1499 Summary, 2017. http://iodp.tamu.edu/scienceops/sitesumm/367_368/367_ss1499.html.

Flint, S.S., Hodgson, D.M., Sprague, A.R., Brunt, R.L., van der Merwe, W.C., Figueiredo, J., Prelat, A., Box, D., Di Celma, C., Kavanagh, J.P. Depositional architecture and sequence stratigraphy of the Karoo basin floor to shelf edge succession, Laingsburg depocentre, South Africa. Marine and Petroleum Geology, 2011, 28(3): 658-674.

Gard, G., Crux, J.A. Reworked Jurassic-Neogene calcareous nannofossils in the central Arctic. Marine Geology, 1994, 119(3-4): 287-300.

Gong, C.L., Wang, Y.M., Zhu, W.L., Li, W.G., Xu, Q. Upper Miocene to Quaternary unidirectionally migrating deep-water channels in the Pearl River Mouth Basin, northern South China Sea. AAPG Bulletin, 2013, 97(2): 285-308.

Haq, B.U. Sequence stratigraphy, sea-level change, and significance for the deep sea. International Association of Sedimentologists, Special Publication, 1991, 12: 3-39.

Hampton, M.A., Lee, H.J., Locat, J. Submarine landslides. Reviews of Geophysics, 1996, 34(1): 33-59.

Hardenbol, J., Caron, M., Amédro, F., Dupuis, C., Robaszynski, F. The Cenomanian-Turonian boundary in central Tunisia in the context of a sequence-stratigraphic interpretation. Cretaceous Research, 1993, 14(4-5): 449-454.

He, Y., Zhang, G.F., Wang, L.L., Kuang, Z.G. Characteristics and occurrence of submarine canyon-associated landslides in the middle of the northern continental slope, South China Sea. Marine and Petroleum Geology, 2014, 57(2): 546-560.

Huang, W., Wang, P.X. Sediment mass and distribution in the South China Sea since the Oligocene. Science in China Series D: Earth Sciences, 2006, 49(11): 1147-1155.

Huang, W., Wang, P.X. Statistics of sediment mass in the South China Sea: Method and results. Frontiers of Earth Science in China, 2007, 1(1): 88-96.

Hubbard, S.M., Ruig, M.J.D., Graham, S.A. Confined channel-levee complex development in an elongate depo-center: Deep-water Tertiary strata of the Austrian Molasse basin. Marine and Petroleum Geology, 2009, 26(1): 85-112.

Hüneke, H., Mulder, T. Deep-sea sediments. Developments in Sedimentology, 63. Elsevier: Amsterdam, 2011, pp, 849.

Jiang, J., Shi, H.S., Lin, C.S., Zhang, Z.T., Wei, A., Zhang, B., Shu, L.F., Tian, H.X., Tao, Z., Liu, H.Y. Sequence architecture and depositional evolution of the Late Miocene to quaternary northeastern shelf margin of the South China Sea. Marine and Petroleum Geology, 2017, 81: 79-97.

Johnson, S.D., Flint, S., Hinds, D., Wickens, H.D.V. Anatomy, geometry and sequence stratigraphy of basin floor to slope turbidite systems, Tanqua Karoo, South Africa. Sedimentology, 2001, 48: 987-1023.

Lericolais, G., Bourget, J., Popescu, I., Jermannaud, P., Mulder, T., Jorry, S., Panin, N. Late Quaternary deep-sea sedimentation in the western Black Sea: New insights from recent coring and seismic data in the deep basin. Global and Planetary Change, 2013, 103: 232-247.

Li, C.F., Xu, X., Lin, J., Sun, Z., Zhu, J., Yao, Y.J., Zhao, X.X., Liu, Q.S., Kulhanek, D.K., Wang, J., Song, T.R., Zhao, J.F., Qiu, N., Guan, Y.X., Zhou, Z.Y., Williams, T., Bao, R., Briais, A., Brown, E.A., Chen, Y.F., Clift, P.D., Colwell, F.S., Dadd, K.A., Ding, W.W., Almeida, I.H., Huang, X.L., Hyun, S., Jiang, T., Koppers, A.A.P., Liu, Q.Y., Liu, C.L., Liu, Z.F., Nagai, R.H., Peleo-Alampay, A., Su, X., Tejada, M.L.G., Trinh, H.S., Yeh, Y.C., Zhang, C.L., Zhang, F., Zhang, G.L. Ages and magnetic structures of the South China Sea constrained by deep tow magnetic surveys and IODP Expedition 349. Geochemistry, Geophysics, Geosystems, 2014, 15: 4958-4983.

Li, H., Wang, Y.M., Zhu, W.L., Xu, Q., He, Y.B., Tang, W., Zhou, H.T., Wang, D., Wu, J.P., Li, D. Seismic characteristics and processes of the Plio-Quaternary unidirectionally migrating channels and contourites in the northern slope of the South China Sea. Marine and Petroleum Geology, 2013, 43: 370-380.

Li, L., Lei, X.H., Zhang, X., Zhang, G.X. Heat flow derived from BSR and its implications for gas hydrate stability zone in Shenhu Area of northern South China Sea. Marine Geophysical Research, 2012, 33(1): 77-87.

Lin, C.S., Jiang, J., Shi, H.S., Zhang, Z.T., Liu, Y.J., Qin, C.G., Li, H., Ran, H.J., Wei. A., Tian, H.X., Xing, Z.C., Yao, Q. Sequence architecture and depositional evolution of the northern continental slope of the South China Sea: Responses to tectonic processes and changes in sea level. Basin Research, 2018, 30: 568-595.

Liu, C.L., Ye, Y.G., Meng, Q.G., He, X.L., Lu, H.L., Zhang, J., Liu, J., Yang, S.X. The Characteristics of gas hydrates recovered from Shenhu Area in the South China Sea. Marine Geology, 2012, 307-310(3): 22-27.

Liu, Z.F., Li, C.F., Kulhanek, D. Preface: Evolution of the deep South China Sea: Integrated IODP expedition 349 results. Marine Geology, 2017, 394: 1-3.

Loutit, T.S., Pisias, N.G., Kennett, J.P. Pacific Miocene carbon isotope stratigraphy using benthic foraminifera. Earth and Planetary Science Letters, 1983, 66: 48-62.

Lü, C.L., Yao, Y.J., Gong, Y.H., Wu. S.G., Li, X.J. Deepwater canyons reworked by bottom currents: sedimentary evolution and genetic model. Journal of Earth Science, 2012, 23(5): 731-743.

Lüdmann, T., Wong, H.K., Wang, P.X. Plio-Quaternary sedimentation process and neotectonics of the northern continental margin of the South China Sea. Marine Geology, 2001, 172(3-4): 331-358.

Ma, B.J., Wu, S.G., Sun, Q.L., Mi, L.J., Wang, Z.Z., Tian, J. The late Cenozoic deep-water channel system in the Baiyun Sag, Pearl River Mouth Basin: development and tectonic effects. Deep Sea Research Part II: Topical Studies in Oceanography, 2015, 122: 226-239.

Macauley, R.V., Hubbard, S.M. Slope channel sedimentary processes and stratigraphic stacking, Cretaceous Tres Pasos Formation slope system, Chilean Patagonia. Marine and Petroleum Geology, 2013, 41: 146-162.

Mayall, M., Jones, E., Casey, M. Turbidite channel reservoirs—Key elements in facies prediction and effective development. Marine and Petroleum Geology, 2006, 23(8): 821-841.

Miller, K.G., Browning, J.V., Aubry, M.P., Wade, B.S., Katz, M E., Kulpecz, A.A., Wright, J.D. Eocene-Oligocene global climate and sea-level changes: St. Stephens Quarry, Alabama. Geological Society of America Bulletin, 2008, 120: 34-53.

Mills, P.C. Genesis and diagnostic value of soft-sediment deformation structures—A review. Sedimentary Geology, 1983, 35(2): 83-104.

Moscardelli, L., Wood, L. New classification system for mass transport complexes in offshore Trinidad. Basin Research, 2008, 20(1): 73-98.

Pang, X., Chen, C.M., Peng, D.J., Zhu, M., Shu, Y., He, M., Shen, J., Liu, B.J. Sequence Stratigraphy of Deep-water Fan System of Pearl River, South China Sea. Earth Science Frontiers, 2007, 14(1): 220-229.

Passega, R. Grain size representation by Cm Patterns as a geological tool. Journal of Sedimentary Research, 1964, 34(4): 830-847.

Patruno, S., Helland-Hansen, W. Clinoform systems: Review and dynamic classification scheme for shorelines, subaqueous deltas, shelf edges and continental margins. Earth-Science Reviews, 2018, 185: 202-233.

Qiao, S.H., Su, M., Kuang, Z.G., Yang, R., Liang, J.Q., Wu, N.Y. Canyon-related undulation structures in the Shenhu area, northern South China Sea. Marine Geophysical Researches,

2015, 36(2-3): 243-252.

Rahman, A. Reworked nannofossils in the North Atlantic Ocean and subpolar basins: Implications for Heinrich events and ocean circulation. Geology, 1995, 23(6): 487-490.

Ru, K., Pigott, J.D. Episodic rifting and subsidence in the South China Sea. AAPG Bulletin, 1986, 70(9): 1136-1155.

Stow, D.A.V., Mayall. Deep-water sedimentary systems: New models for the 21st century. Marine and Petroleum Geology, 2000, 17(2): 125-135.

Su, M., Sha, Z.B., Qiao, S.H., Yang, R., Wu, N.Y., Cong, X.R., Liu, J. Sedimentary evolution since Quaternary in the Shenhu hydrate drilling area, northern South China Sea. Chinese Journal of Geophysics, 2015, 58(8): 2975-2985. (in Chinese with English abstract)

Su, M., Yang, R., Wang, H.B., Sha, Z.B., Liang, J.Q., Wu, N.Y., Qiao, S.H., Cong, X.R. Gas hydrates distribution in the Shenhu Area, northern South China Sea: comparisons between the eight drilling sites with gas-hydrate petroleum system. Geological Acta, 2016, 14(2): 79-100.

Su, Z., Cao, Y.C., Wu, N.Y., Chen, D.F., Yang, S.X., Wang, H.B. Numerical investigation on methane hydrate accumulation in Shenhu Area, northern continental slope of South China Sea. Marine and Petroleum Geology, 2012, 38(1): 158-165.

Sun, Y.B., Wu. S.G., Dong, D.D., Lüdmann, T., Gong, Y.H. Gas hydrates associated with gas chimneys in fine-grained sediments of the northern South China Sea. Marine Geology, 2012, 311-314: 32-40.

Ujiié, H. Early Pleistocene birth of the Okinawa Trough and Ryukyu Island Arc at the northwestern margin of the Pacific: evidence from Late Cenozoic planktonic foraminiferal zonation. Palaeogeography Palaeoclimatology Palaeoecology, 1994, 108(3-4): 457-474.

Van Wagoner, J.C., Mitchum, R.M., Posamentier, H.W., Vail, P.R. An overview of sequence stratigraphy and key definitions. In: Bally, A.W. (Ed.), Atlas of Seismic Stratigraphy, volume 1. Studies in Geology, vol. 27. American Association of Petroleum Geologists, 1987, pp. 11-14.

Van Wagoner, J.C., Mitchum Jr., R.M., Campion, K.M., Rahmanian, V.D. Siliciclastic sequence stratigraphy in well logs, core, and outcrops: concepts for high-resolution correlation of time and facies. American Association of Petroleum Geologists Methods in Exploration Series, 1990, vol. 7, pp. 55.

Vanneste, K., Verbeeck, K., Petermans, T. Pseudo-3D imaging of a low-slip-rate, active normal fault using shallow geophysical methods: The Geleen fault in the Belgian Maas River valley. Geophysics, 2008, 73: B1-B9.

Wang, P.X., Prell, W.L., Blum, P., Baldauf, J. Proceedings of the Ocean Drilling Program, Initial Reports South China Sea, vol. 184, 2000, 1-77.

Wang, X.J., Wu, S.G., Lee, M., Guo, Y.Q., Yang, S.X., Liang, J.Q. Gas hydrate saturation from acoustic impedance and resistivity logs in the Shenhu area, South China Sea. Marine and Petroleum Geology, 2011a, 28(9): 1625-1633.

Wang, X.J., Hutchinson, D.R., Wu, S.G., Yang, S.X., Guo, Y.Q. Elevated gas hydrate saturation within silt and silty clay sediments in the Shenhu area, South China Sea. Journal of Geophysical Research, 2011b, 116: B05102.

Wang, X.J., Lee, M., Collett, T., Yang, S.X., Guo, Y.Q., Wu, S.G. Gas hydrate identified in sand-rich inferred sedimentary section using downhole logging and seismic data in Shenhu area, South China Sea. Marine and Petroleum Geology, 2014a, 51(2): 298-306.

Wang, X.J., Collett, T.S., Lee, M.W., Yang, S.X., Guo, Y.Q., Wu, S.G. Geological controls on the occurrence of gas hydrate from core, downhole log, and seismic data in the Shenhu area, South China Sea. Marine Geology, 2014b, 357: 272-292.

Wang, X., Qian, J., Collett, T. S., Shi, H.S., Yang, S.X., Yan, C.Z., Li. Y.P., Wang, Z.Z., Chen, D.X. Characterization of gas hydrate distribution using conventional 3D seismic data in the Pearl River Mouth Basin, South China Sea. Interpretation, 2016, 4(1): SA25-SA37.

Wu, N.Y., Yang, S.X., Zhang, H.Q., Liang, J.Q., Wang, H.B., Su, X., Fu, S.Y. Preliminary discussion on natural gas hydrate reservoir system of Shenhu area, North Slope of South China Sea. 6th International Conference on Gas Hydrates (ICGH 2008), 7 pp, Worldoils, Vancouver B C, Canada, 6-10 Jul, 2008.

Wu, S.G., Dong, D.D., Yang, S.X., Zhang, G.X., Wang, Z.J., Li, Q.P., Liang, J.Q., Gong, Y.H., Sun, Y.B. Genetic model of the hydrate system in the fine grain sediments in the northern continental slope of South China Sea. Chinese Journal of Geophysics, 2009, 52(7): 1849-1857. (in Chinese with English abstract)

Yang, R., Su, M., Qiao, S.H., Cong, X.R., Su, Z., Liang, J.Q., Wu, N.Y. Migration of methane associated with gas hydrates of the Shenhu Area, northern slope of South China Sea. Marine Geophysical Research, 2015, 36(2-3): 253-261.

Yang, S.X., Zhang, H.Q., Wu, N.Y., Su, X., Schultheiss, P., Holland, M., Zhang, G.X., Liang, J.Q., Lu, J.A., Rose, K. High concentration hydrate in disseminated forms obtained in Shenhu area, North Slope of South China Sea. 6th International Conference on Gas Hydrates (ICGH 2008), 10 pp, Worldoils, Vancouver B C, Canada, 6-10 Jul, 2008.

Yang, S.X., Zhang, M., Liang, J.Q., Lu, J.A., Zhang, Z.J., Holland, M., Schultheiss, P., Fu, X.Y., Sha, Z.B., the GMGS3 Science Team. Preliminary results of China's third Gas hydrate drilling expedition: a Critical step from discovery to development in the South China Sea. Fire in the ice, 2015a, 15(2): 1-6.

Yoon, S.H., Chough, S.K., Park, S.J. Sequence model and its application to a Miocene shelf-slope system in the tectonically active Ulleung Basin margin, East Sea (Sea of Japan). Marine and Petroleum Geology, 2003, 20(10): 1089-1103.

Yu, X.H., Wang, J.Z., Liang, J.Q., Li, S.L., Zeng, X.M., Li, W. Depositional characteristics and accumulation model of gas hydrates in northern South China Sea. Marine and Petroleum Geology, 2014, 56(3): 74-86.

Zhang, P.Z., Molnar, P., Downs, W.R., Increased sedimentation rates and grain sizes 2–4 Myr ago due to the influence of climate change on erosion rates. Nature, 2001, 410(6831): 891-897.

Zhou, D., Sun, Z., Liao, J., Zhao, Z.X., He, M., Wu, X.J., Pang, X. Filling history and post-breakup acceleration of sedimentation in Baiyun Sag, deepwater northern South China Sea. Journal of Earth Science, 2009, 20(1): 160-171.

Zhou, W., Wang, Y.M., Gao, X.Z., Zhu, W.L., Xu, Q., Xu, S., Cao, J.Z., Wu, J. Architecture, evolution history and controlling factors of the Baiyun submarine canyon system from the middle Miocene to Quaternary in the Pearl River Mouth Basin, northern South China Sea. Marine and Petroleum Geology, 2015, 67: 389-407.

Zhu, M.Z., Graham, S., Pang, X., McHargue, T. Characteristics of migrating submarine canyons from the middle Miocene to present: Implications for paleoceanographic circulation, northern South China Sea. Marine and Petroleum Geology, 2010, 27(1): 307-319.

Zhu, W.L., Huang, B.J., Mi, L.J., Wilkins, R.W.T., Fu, N., Xiao, X.M. Geochemistry, origin, and deep-water exploration potential of natural gases in the Pearl River Mouth and Qiongdongnan basins, South China Sea. AAPG Bulletin, 2009, 93(6): 741-761.

Zhu, Y.H., Huang, X., Fu, S.Y., Su, P.B. Gas sources of natural gas hydrates in the Shenhu Drilling Area, South China Sea: Geochemical evidence and geological analysis. Acta Geologica Sinica (English Edition), 2013, 87(3): 767-776.

Figures and table captions

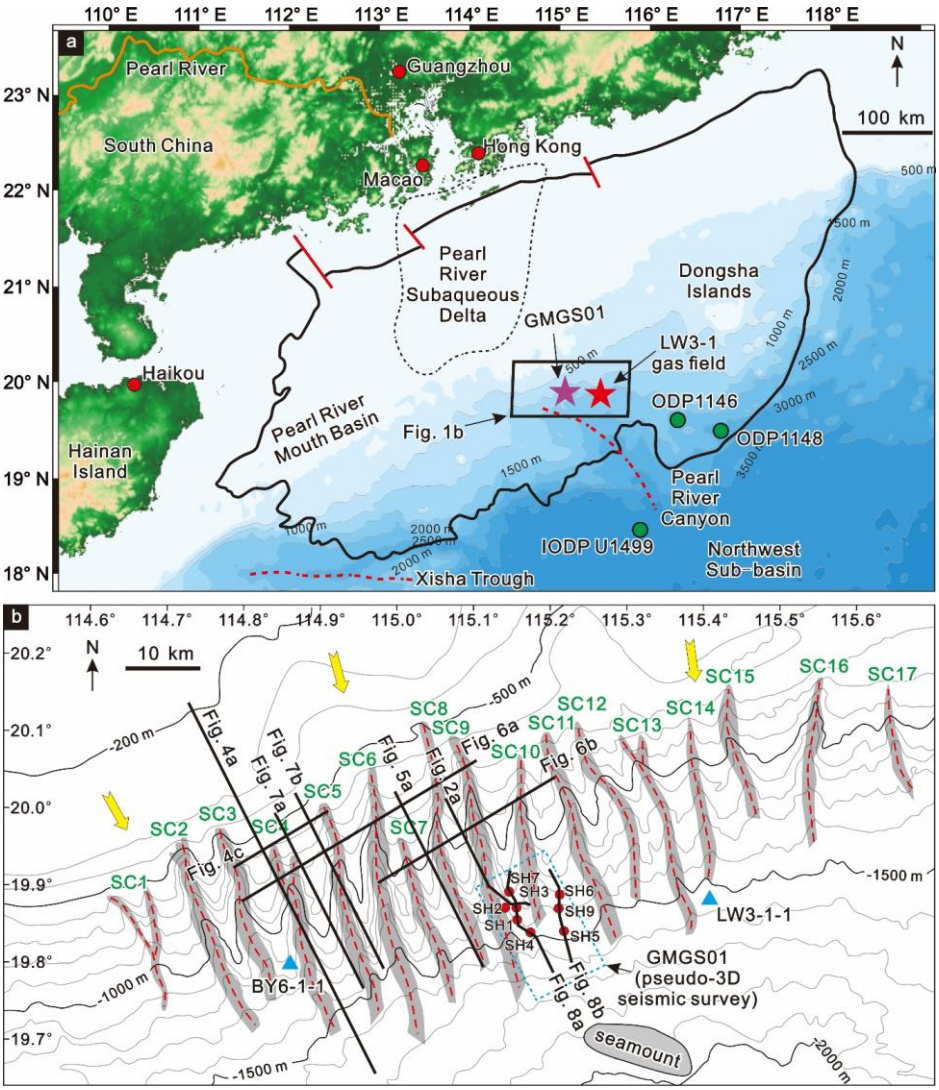

Figure 1. (a) Regional bathymetric map showing the location of the Pearl River Mouth Basin (PRMB); see black solid line. The interval between bathymetric contours is 500 m. The Pearl River Subaqueous Delta is shown by the dotted black line (after Chen et al., 2014). The red and violet stars represent the LW3-1 deep-water gas field and target areas for gas hydrates drilled during expedition GMGS01. The locations of ODP Sites 1146 and 1148, and IODP Site U1499 are shown by the green solid circles. The axes of the Xisha Trough and Pearl River Canyon are shown by the red dotted lines. The small box shows the relative location of Figure 1b below. (b) Bathymetric map showing the location of seventeen (17) slope-confined submarine canyons in grey. Contour interval in this figure is 100 m. The red dotted lines mark the axes of discrete canyons. The eight (8) drilling sites completed by the Guangzhou Marine Geological Survey (GMGS) in 2007 are shown as red circles. Two wells LW3-1-1 and BY6-1-1 (see blue triangles) were drilled by the Chinese National Offshore Oil Corporation (CNOOC) in this same area. The box with the blue dotted line is the pseudo-3D seismic survey competed during expedition GMGS01. Yellow arrows indicate the direction of possible terrestrial sediment sourced from the Pearl River Subaqueous Delta. This interpreted direction of sediment flow is roughly parallel to the orientation of submarine canyons on the continental slope. SC: submarine canyon.

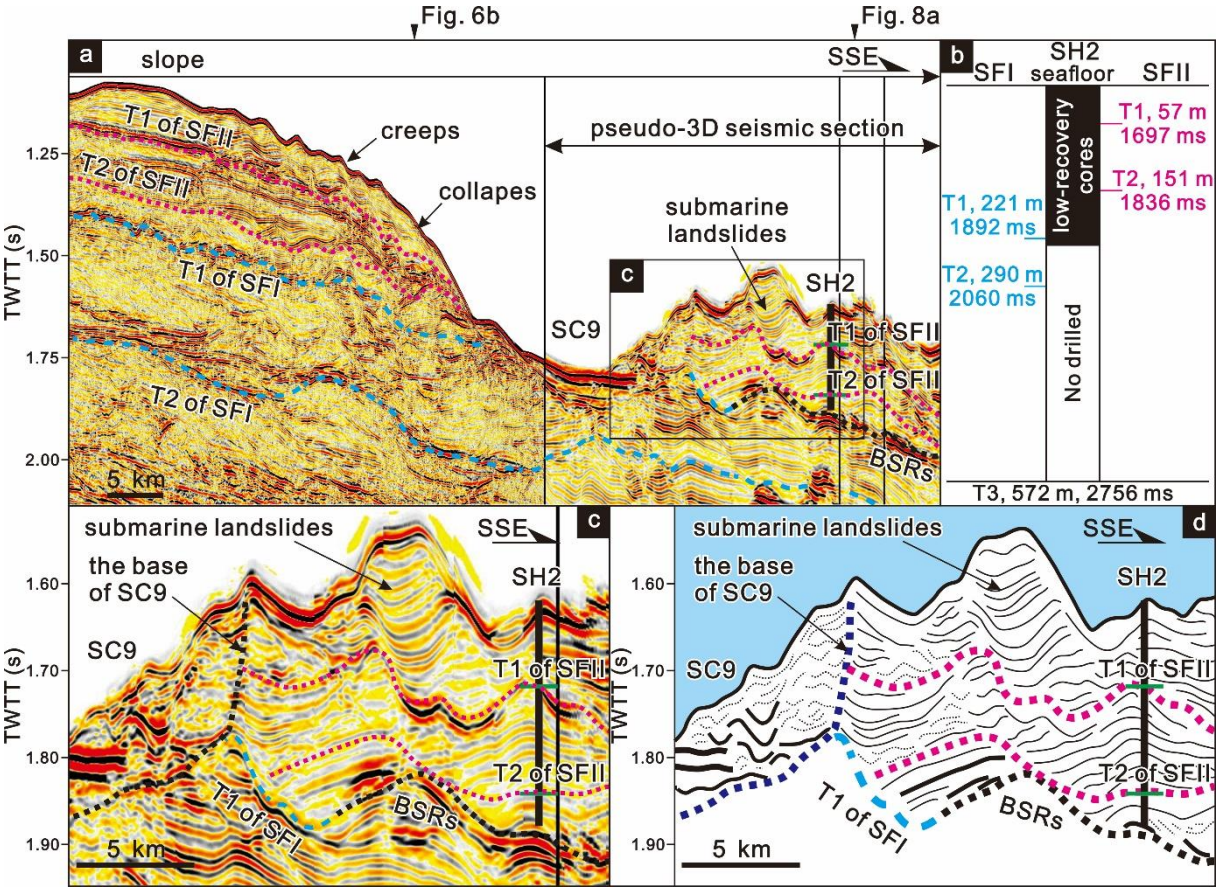

Figure 2. (a) SSE-striking seismic profile crossing submarine canyon 9 (SC9) from the upper to the lower continental slope. A pseudo-3D seismic section intersects the southern part of this profile. Drilling site SH2 is located in the intercanyon area between SC9 and SC10. Stratigraphic boundaries T1 and T2, based on both SFI and SFII, are shown in this seismic profile as blue and magenta dotted lines, respectively. The black dotted line highlights the presence of bottom simulating reflectors (BSRs). (b) Schematic diagram comprising the depths of boundaries T1 and T2 in meters (m) and two-way travel time (ms) from SFI and SFII. This diagram shows the different depths of T1 and T2 when considering the two contrasting stratigraphic frameworks SFI and SFII. (c) Zoomed in seismic section crossing hydrate site SH2 to stress that T1 and T2 are untraceable within convoluted strata to the NNW. (d) Line-drawn interpretation of Fig. 2c. The locations of the seismic profile and drilling site SH2 are shown in Fig. 1b. SC: submarine canyon; BSRs: bottom simulating reflectors; TWTT: two-way travel time.

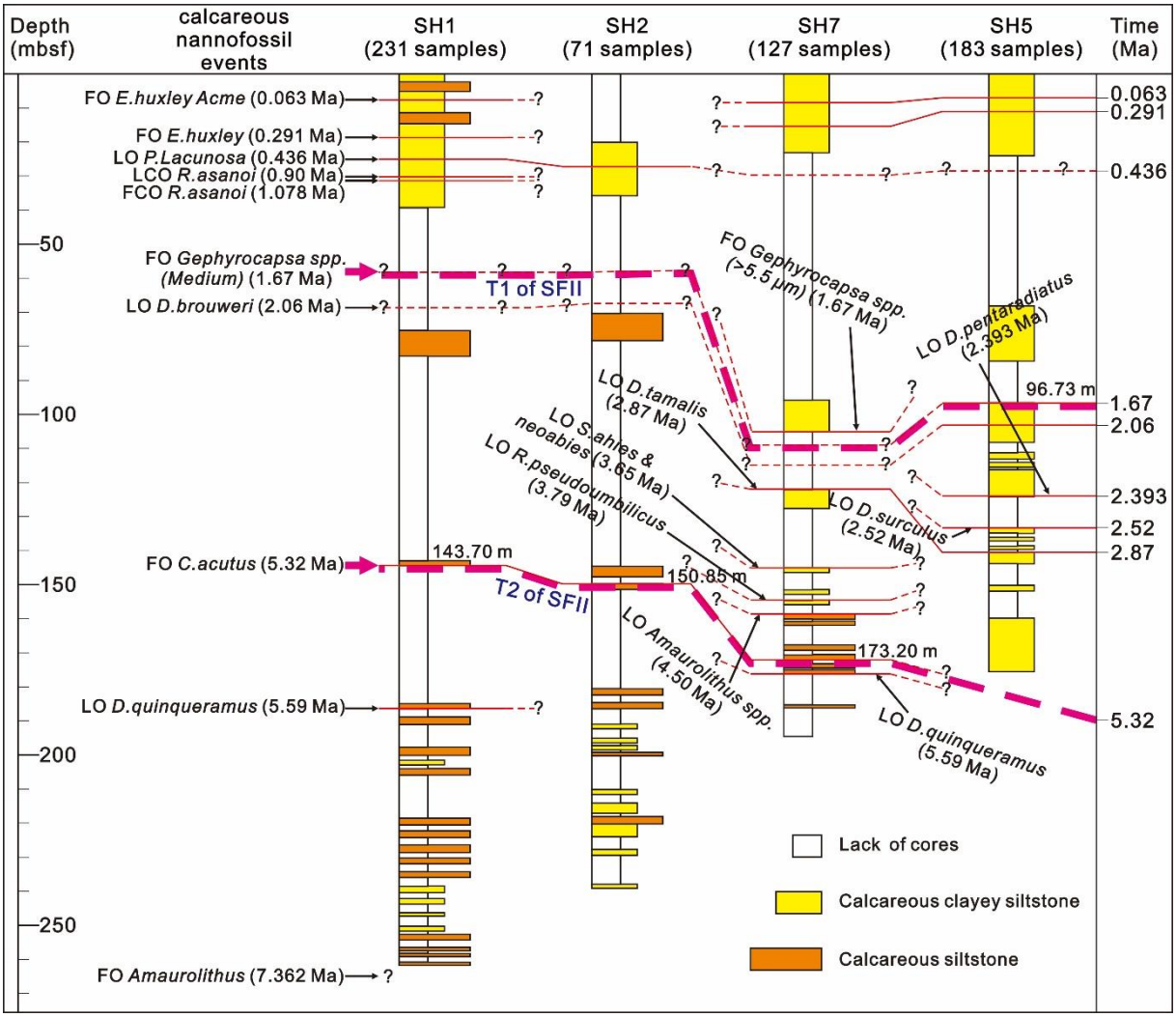

Figure 3. Calcareous nannofossil horizons in sites SH1, SH2, SH5 and SH7 (after Chen et al., 2013). Calcareous siltstones are shown in brown and clayey siltstones in yellow. The magenta dotted lines represent stratigraphic boundaries T1 and T2 of SFII. Red dotted lines with question marks show speculative depths for some of the stratigraphic boundaries considered. FO: first occurrence; LO: last occurrence; FCO: first consistent occurrence; LCO: last consistent occurrence. The locations of the hydrate sites are shown in Fig. 1b.

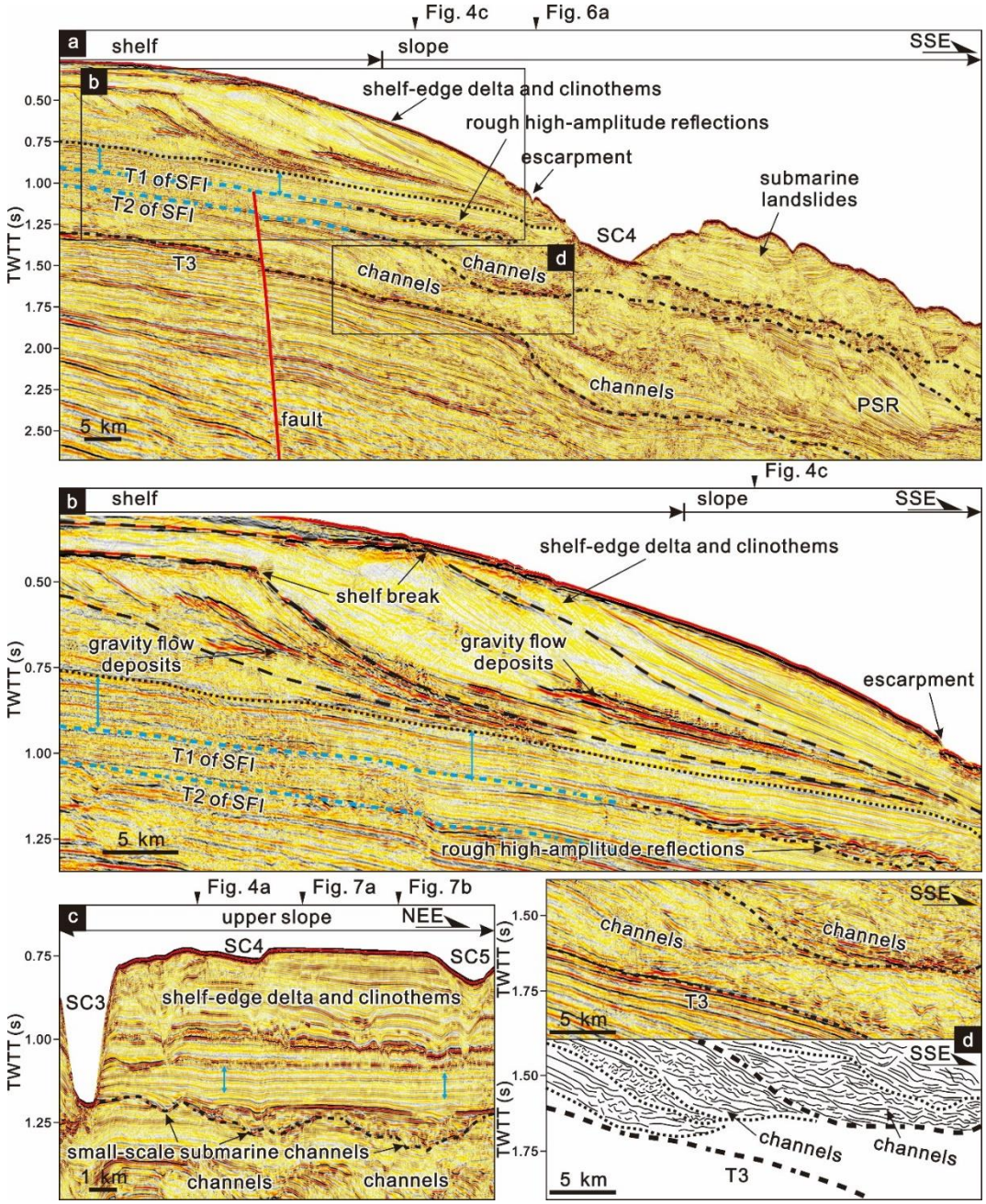

Figure 4. (a) SSE-striking seismic profile showing stratigraphic boundaries T1 and T2 based on SFI. Blue double-headed arrows highlight the isochoric, continuous seismic reflections referred to in the text. On the shelf edge, stratigraphic boundaries T1 and T2 can be traced unequivocally as the bases of isochoric continuous seismic reflections (Li et al., 2013; Zhou et al., 2015; Jiang et al., 2017). At places, these two boundaries correlate with erosional surfaces. (b) Zoomed in section imaging the shelf and shelf edge. Here, prograding complexes can be divided into multiple sub-sequences, some with mass-wasting deposits of high amplitude - as shown in Figure 8 from Jiang et al. (2017). (c) Perpendicular seismic section to Fig. 4a. The irregular high-amplitude reflections in this figure relate to the presence of small-scale submarine channels. (d) Zoomed in section and corresponding interpretation from part of Fig. 4a. The figure shows the characteristic features of submarine channels in Upper Miocene to Pliocene strata.. Location of the seismic profile is shown in Fig. 1b. SC: submarine canyon; TWTT: two-way travel time

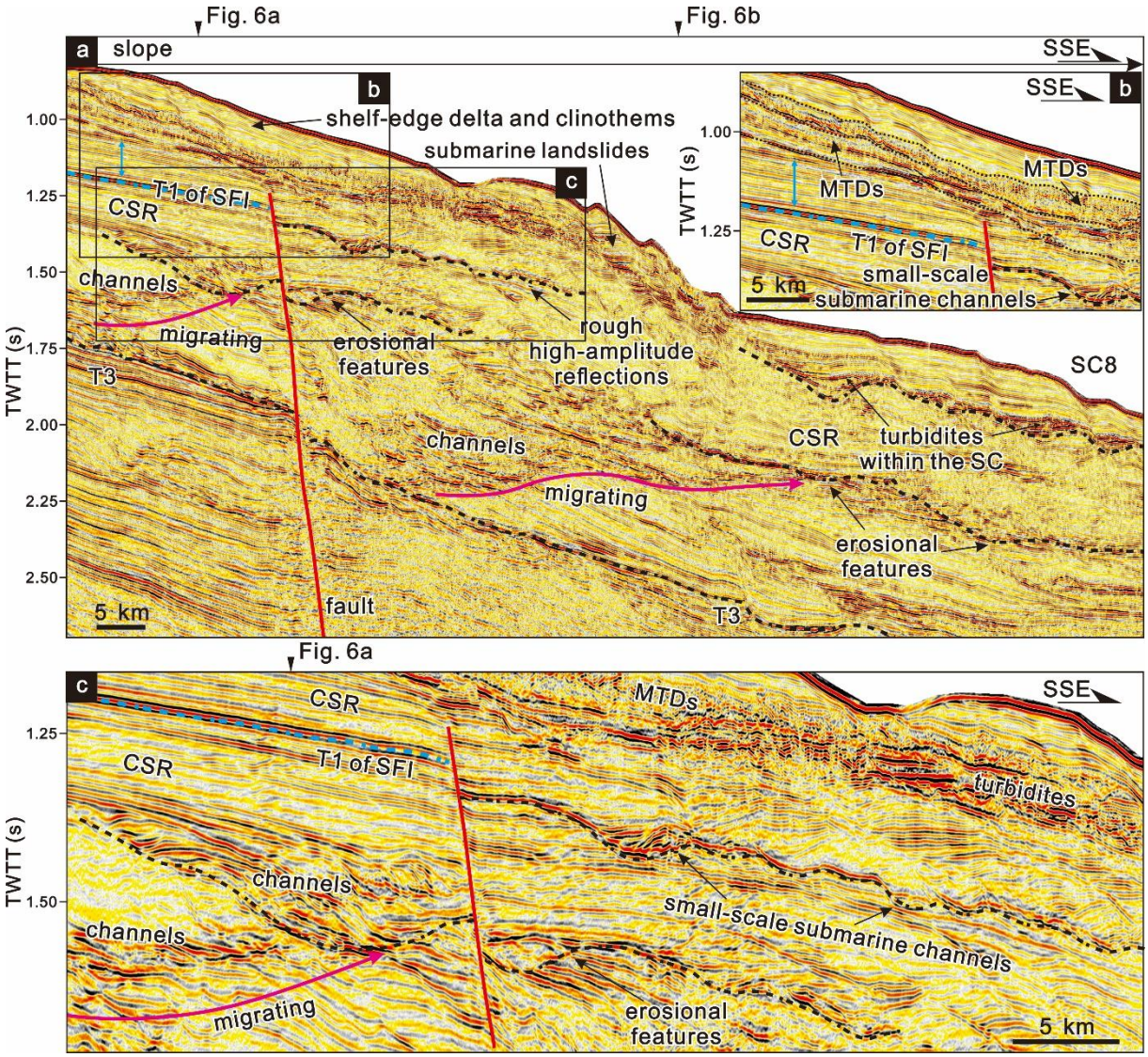

Figure 5. (a) SSE-striking seismic profile across submarine canyon 8 showing characteristic erosional features. Irregular high-amplitude seismic reflections are obvious on the upper and middle continental slope, corresponding to the base of isochoric continuous moderate-amplitude reflections (see blue double-headed arrow) at the shelf edge. In the intracanyon area of submarine canyon 8, small-scale erosional features are related to the bases of turbidite deposits transported downslope along submarine canyon 8. (b) Zoomed in seismic section from Fig. 5a showing mass-transport deposits (MTDs) with chaotic high-amplitude seismic reflections – an interval likely related to the correlative strata accumulated at the shelf edge in Fig. 4b. (c) Zoomed in seismic section showing irregular high-amplitude reflections interpreted as small-scale submarine channels. Submarine channels in Upper Miocene-Pliocene strata are also observed in this seismic section. The location of the seismic profile is shown in Fig. 1b. MTDs: mass transport deposits; CSR: continuous seismic reflections; SC: submarine canyon; TWTT: two-way travel time.

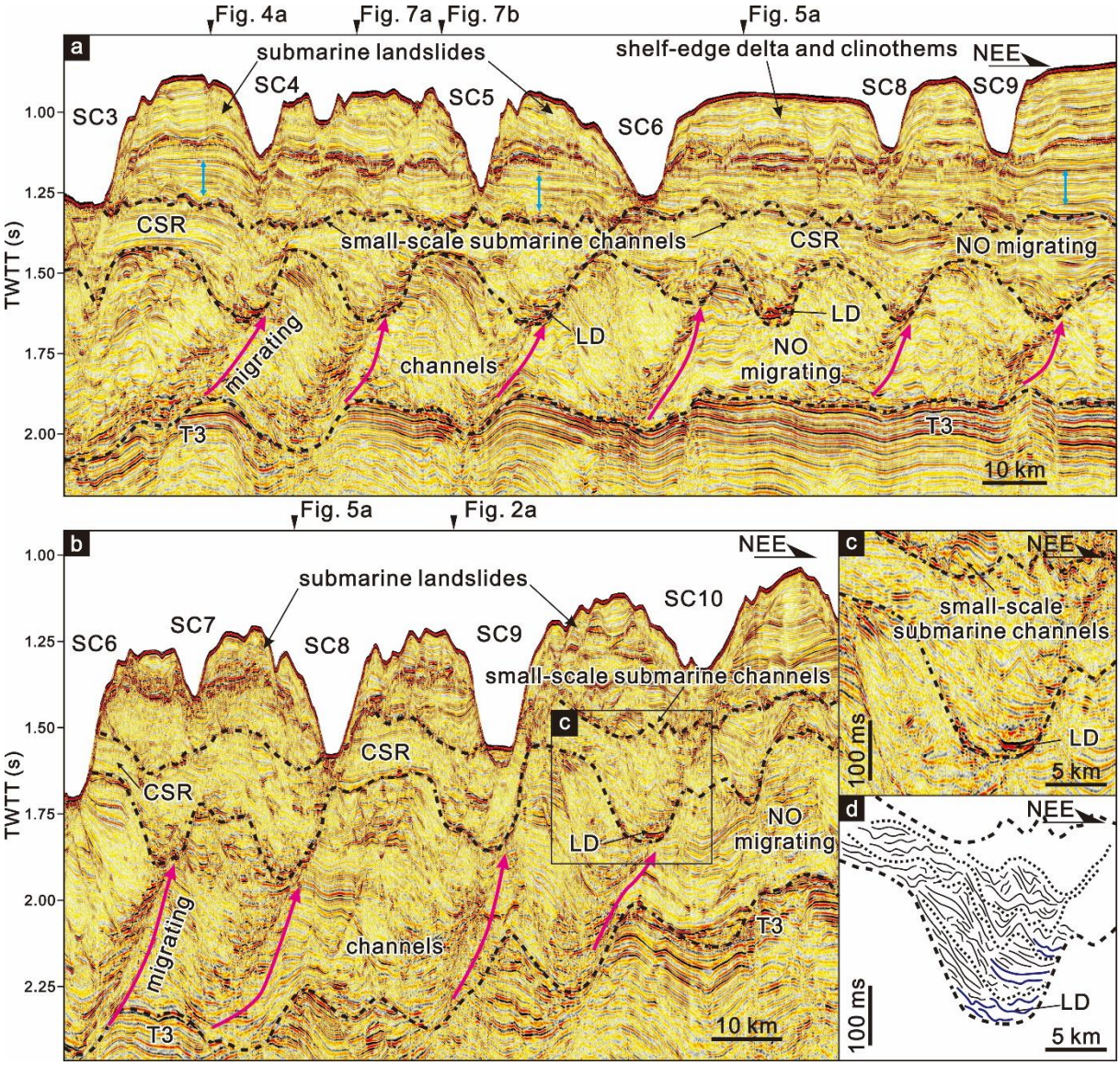

Figure 6. NEE-striking seismic profiles crossing the (a) headwall areas and (b) upper reaches of slope-confined submarine canyons with clear angular unconformities at their bases and flanks. Unidirectionally migrating canyons and channels have developed in the study area since the Late Miocene (stratigraphic boundary T3) as documented by Zhu et al. (2010), Lü et al. (2012), Ding et al. (2013), Gong et al. (2013), Li et al. (2013), Zhou et al. (2015), and Ma et al. (2015). At places, laterally migrating channels show lenticular high-amplitude reflections (channel-lag deposits). Small-scale unconformities are overlain by draping strata with isochoric moderate-amplitude reflections (blue double-headed arrows). (c) Zoomed in seismic profile and (d) corresponding line-drawn interpretation providing more detail on the interpreted channel-lag deposits. The locations of the seismic profiles are shown in Fig. 1b. LD: lag deposits; CSR: continuous seismic reflections; SC: submarine canyon; TWTT: two-way travel time.

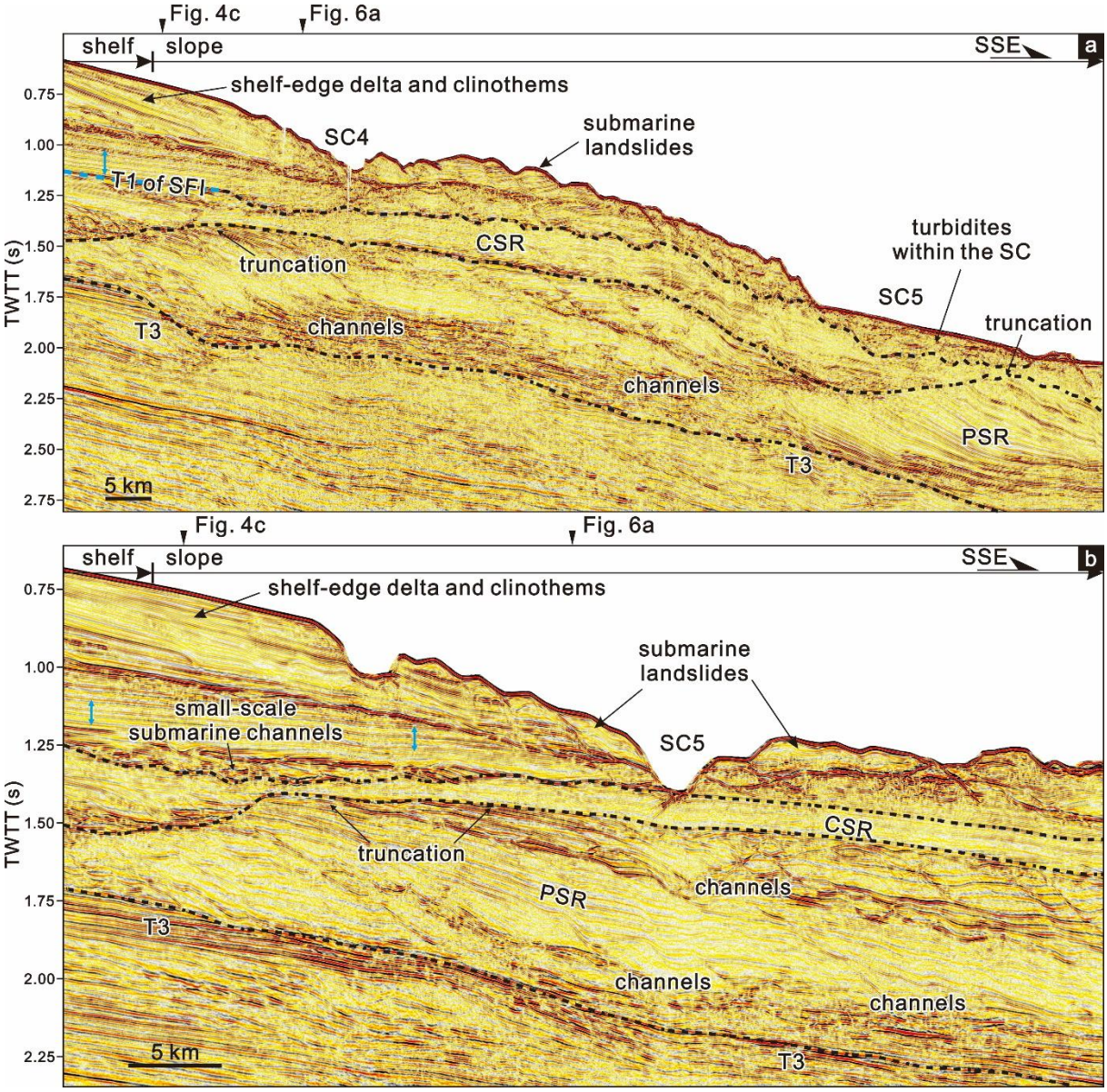

Figure 7. SSE-striking seismic profiles showing key stratigraphic boundaries identified on the middle to lower continental slope, where the erosional power of submarine canyons 4 and 5 was relatively weak. (a) Oblique high-amplitude reflections were truncated and draped in this seismic profile by a set of isochoric, continuous moderate-amplitude reflections. The upper part of the prograding seismic reflections is truncated across the continental slope. (b) Similar erosional truncation on top of prograding seismic reflections occurs together with small-scale submarine channels and erosional surfaces. On the shelf edge and upper continental slope, flat continuous moderate-amplitude seismic reflections below the shelf-edge delta and associated clinothems can also be correlated with small-scale erosional features. The locations of the seismic profiles are shown in Fig. 1b. CSR: continuous seismic reflections; PSR: prograding seismic reflections; SC: submarine canyon; TWTT: two-way travel time.

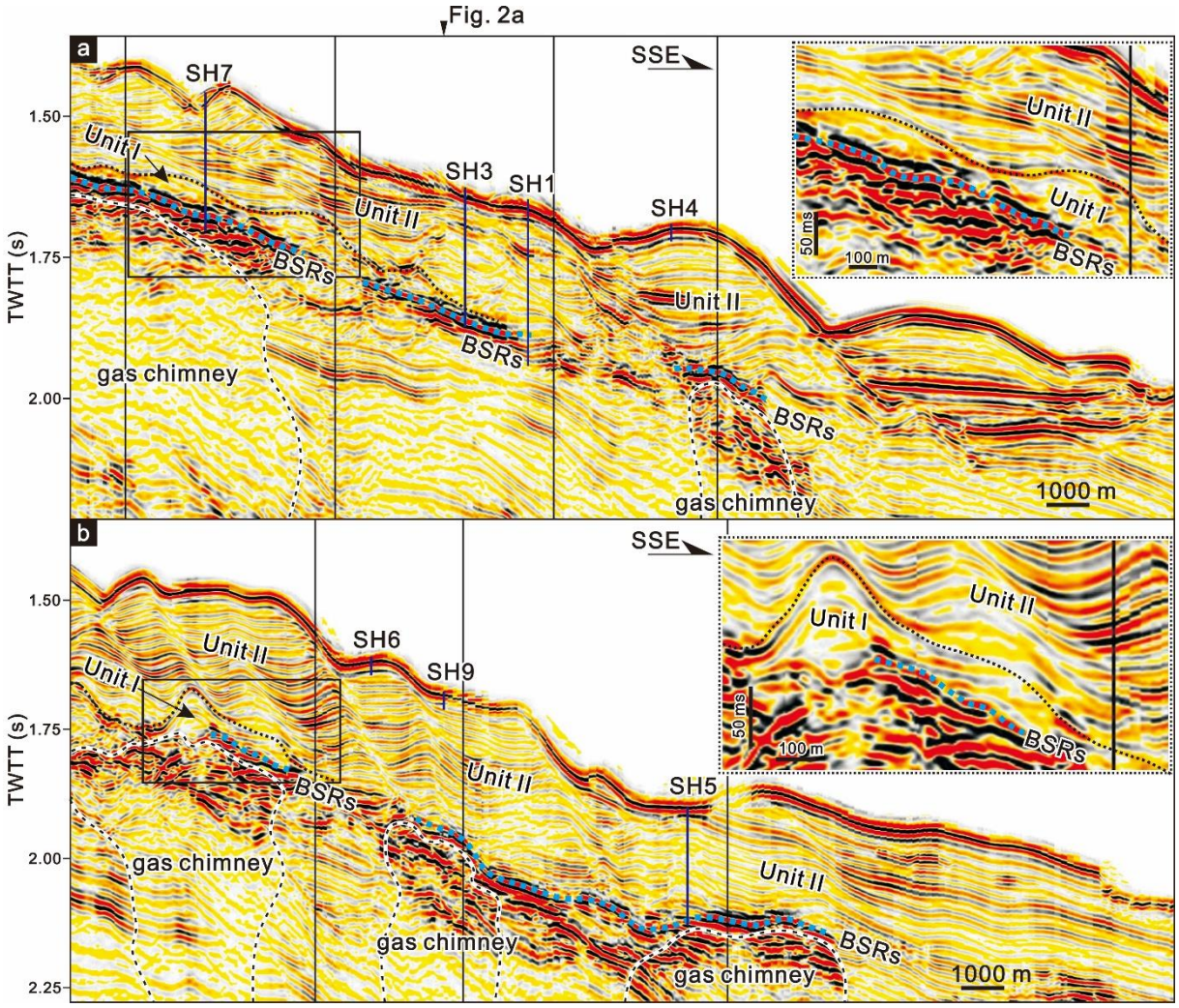

Figure 8. (a) and (b) Pseudo-3D seismic sections across the eight hydrate drilling sites. The sections highlight two units with distinct seismic internal characters above the imaged BSRs. Zoomed in sections (see the two insets) reveal thin-bedded chaotic high-amplitude reflections with lenticular- to irregular-shaped geometries above the BSRs. Moderate-amplitude reflections with wavy geometries occur above the BSRs. The gas chimneys on the 3D seismic sections were studied by Wang et al. (2011b), Sun et al. (2012), Yang et al. (2015) and Chen et al. (2016). Locations of the seismic profiles and drilling sites are shown in Fig. 1b. BSRs: bottom simulating reflectors; TWTT: two-way travel time.

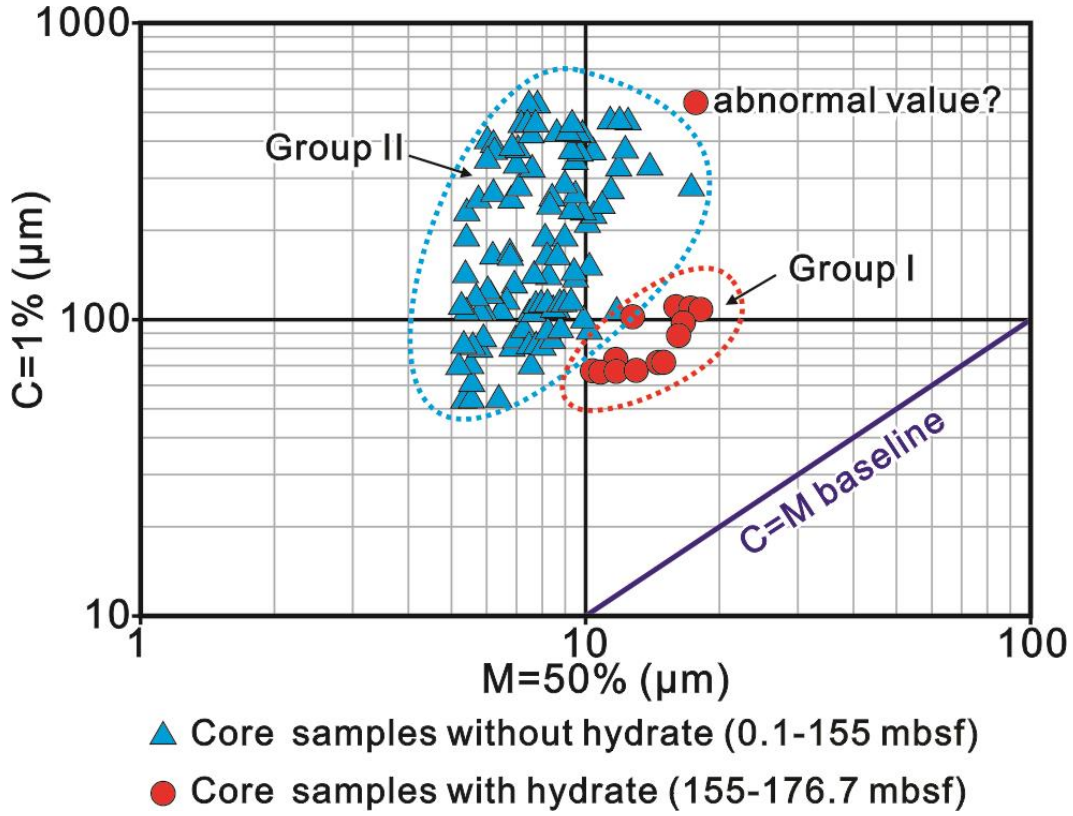

Figure 9. Scatter plot of one-percentile and median values for grain size - the Cm pattern defined by Passega (1964) - at hydrate drilling site SH7. The plot is based on data from 116 samples collected in low-recovery sediment cores from depths of 0.1 to 176.7 mbsf. The location of site SH7 is shown in Fig. 1b.

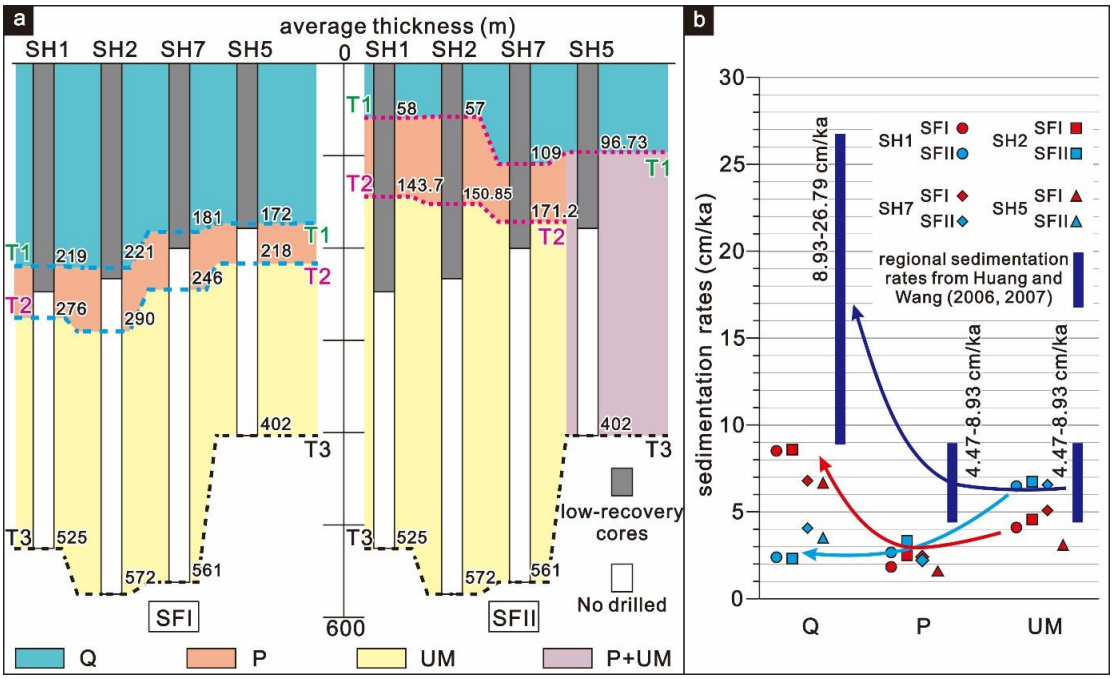

Figure 10. Comparison between the two contrasting stratigraphic frameworks (SFI and SFII) in terms of the (a) average thickness for the three stratigraphic intervals (Quaternary, Pliocene and Upper Miocene from the bottom to the top) and (b) variation trends of average sedimentation rates from Late Miocene to Quaternary at the four hydrate drilling sites of GMGS01. Stratigraphic boundary T2 from SFII was not defined at site SH5 (Chen et al., 2013), and the pink shadow in the Fig. 5a indicates the Pliocene and Upper Miocene intervals. The violet arrow in Fig. 5b shows the variation trends of average sedimentation rates from Late Miocene to Quaternary in the northern slope of the PRMB, as suggested by Huang and Wang (2006, 2007). Q: Quaternary Interval; P: Pliocene Interval; LM: Late Miocene Interval; P+LM: Intervals Pliocene and Late Miocene. Locations of the hydrate drilling sites are shown in Fig. 1b.

Table 1. Comparison between the depths of stratigraphic boundaries T1 and T2 based on the two contrasting schemes SF1 and SFII, at the four gas hydrate drilling sites. Stratigraphic boundary T3 (base of Late Miocene) is documented as the base of migrating channel-fill deposits, whose depth is calculated using a power time-depth function for the PRMB introduced by Zhou et al. (2008). In the target area with gas hydrates (GMGS01), stratigraphic boundary T1 of SFI was traced and coincides with bottom simulating reflectors (BSRs) (Fig. 2a). As a result, the depths of stratigraphic boundary T1 of SFI at hydrate drilling sites could be inferred from the seismic data as shown in Wang et al. (2014b). Based on our seismic data, two-way travel times for stratigraphic boundary T2 of SFI can be obtained and converted into true depths using a power time-depth function for the PRMB introduced by Zhou et al. (2008). The depths of stratigraphic boundaries T1 and T2 of SFII were estimated through analysis of calcareous nannofossil assemblages in Chen et al. (2013). Stratigraphic boundary T2 of SFII was not interpreted at site SH5 due to low recovery of sediment recorded there.

Table 2 Comparisons amongst the calculated average sedimentation rates in Stage 1 (Quaternary), based on the two contrasting schemes SFI and SFII, and published regional data.